

SIT-T-70-002



CIRCULATING COPY
Sea Grant Depository

PREDICTION OF MOTIONS OF
OCEAN PLATFORMS IN OBLIQUE SEAS

by

C. H. Kim and F. Chou

JUNE 1970

DAVIDSON  LABORATORY

OCEAN ENGINEERING

DEPARTMENT

STEVENS INSTITUTE OF TECHNOLOGY

OCEAN ENGINEERING DEPARTMENT
Stevens Institute of Technology
Castle Point Station
Hoboken, New Jersey 07030

Report SIT-0E-70-1

June 1970

PREDICTION OF MOTIONS OF OCEAN PLATFORMS IN OBLIQUE SEAS

by

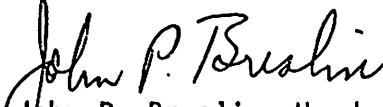
C. H. Kim and F. Chou

This investigation was supported in part by the National Science Foundation, under NSF/Sea Grant GH-60. Requests for copies of the report should be addressed to the Clearinghouse for Scientific and Technical Information, 5285 Port Royal Road, Springfield, Virginia 22151.

(SIT-0E Project 3617/458)

xiii + 78 pp.
1 appendix
17 figures

Approved


John P. Breslin, Head
Department of Ocean Engineering

ABSTRACT

This report presents a new procedure for predicting the motions of some ocean platforms in oblique waves. Frank's method of calculating hydrodynamic forces and moments on oscillating cylinders is extended not only to the calculation of hydrodynamic moment arms but also to the calculation of wave-exciting forces and moments on a restrained ocean platform in oblique waves. The coupled vertical and lateral equations of motion are applied in determining the important motions of ocean-platform models of the ship and jackup type, in oblique seas. The predictions are in good agreement with the experimental results.

KEYWORDS

Hydrodynamic Forces
Wave-Exciting Forces
Motions of Ocean Platforms

CONTENTS

Abstract	iii
List of Figures	vii
Nomenclature	ix
INTRODUCTION	1
HYDRODYNAMIC FORCES AND MOMENTS ON CYLINDERS OSCILLATING IN CALM WATER	3
WAVE-EXCITING FORCES AND MOMENTS ON A RESTRAINED BODY IN OBLIQUE SEAS	7
COUPLED EQUATIONS OF MOTION IN OBLIQUE SEAS	15
Coupled Heaving and Pitching Equations	15
Coupled Swaying, Yawing, and Rolling Equations	17
MOTION OF A SHIP-SHAPED PLATFORM IN OBLIQUE SEAS	21
Model and Model Test Condition	21
Coupled Heaving and Pitching Motions	22
Coupled Swaying, Yawing, and Rolling Motions	23
MOTION OF JACKUP RIG MODEL IN OBLIQUE SEAS	27
Model and Model Test Conditions	27
Test Procedure	28
Heaving, Pitching, and Surging Motions	28
Heaving, Swaying, Yawing, and Rolling Motions	30
CONCLUSIONS AND RECOMMENDATIONS	31
ACKNOWLEDGEMENTS	33
REFERENCES	35
FIGURES 1-17	37-75
APPENDIX	77

LIST OF FIGURES

1A. Strip Section	37
1B. Coordinate Systems	38
1C. Definition of Forces and Motions	39
2. Heaving and Pitching Inertial and Damping Coefficients of Ship Model	40
3. Heave- and Pitch-Exciting Force and Moment on Ship Model in Beam Seas ($\mu = 90^\circ$)	41
4A. Heaving Motion of Ship Model in Beam Seas ($\mu = 90^\circ$)	42
4B. Pitching Motion of Ship Model in Beam Seas ($\mu = 90^\circ$)	43
5A. Heave-Exciting Force on Ship Model in Oblique Seas	44
5B. Pitch-Exciting Moment on Ship Model in Oblique Seas	45
6A. Heaving Motion of Ship Model in Oblique Seas	46
6B. Pitching Motion of Ship Model in Oblique Seas	47
7A. Swaying and Yawing Inertial and Damping Coefficients of Ship Model	48
7B. Rolling Inertial and Linear and Non-Linear Damping Coefficients of Ship Model	49
7C. Coupling Inertial and Damping Coefficients of Ship Model	50
8A. Sway- and Yaw-Exciting Force and Moment on Ship Model in Beam Seas ($\mu = 90^\circ$)	51
8B. Roll-Exciting Moment on Ship Model in Beam Seas ($\mu = 90^\circ$)	52
9A. Swaying Motion of Ship Model in Beam Seas ($\mu = 90^\circ$)	53
9B. Yawing Motion of Ship Model in Beam Seas ($\mu = 90^\circ$)	54
9C. Rolling Motion of Ship Model in Beam Seas ($\mu = 90^\circ$)	55
9D. Effect of the Wave Slope on the Roll Motions in Beam Seas ($\mu = 90^\circ$)	56

List of Figures (cont'd)

10A.	Sway-Exciting Force on Ship Model in Oblique Seas	57
10B.	Yaw-Exciting Moment on Ship Model in Oblique Seas	58
10C.	Roll-Exciting Moment on Ship Model in Oblique Seas	59
11A.	Swaying Motion of Ship Model in Oblique Seas	60
11B.	Yawing Motion of Ship Model in Oblique Seas	61
11C.	Rolling Motion of Ship Model in Oblique Seas	62
12A.	Photograph of Jackup Rig Model with Legs Down	63
12B.	Photograph of Jackup Rig Model with Legs Up in Waves	63
13A.	Heaving Motion of Jackup Rig Model in Head Seas	64
13B.	Pitching Motion of Jackup Rig Model in Head Seas	65
13C.	Surging Motion of Jackup Rig Model in Head Seas	66
14A.	Surging Motion of Jackup Rig Model in Quartering Seas ($\mu = 45^\circ$)	67
14B.	Pitching Motion of Jackup Rig Model in Quartering Seas ($\mu = 45^\circ$)	68
15A.	Heaving Motion of Jackup Rig Model in Beam Seas ($\mu = 90^\circ$) . . .	69
15B.	Swaying Motion of Jackup Rig Model in Beam Seas ($\mu = 90^\circ$) . . .	70
15C.	Rolling Motion of Jackup Rig Model in Beam Seas ($\mu = 90^\circ$) . . .	71
16A.	Swaying Motion of Jackup Rig Model in Quartering Seas ($\mu = 45^\circ$)	72
16B.	Yawing Motion of Jackup Rig Model in Quartering Seas ($\mu = 45^\circ$)	73
16C.	Rolling Motion of Jackup Rig Model in Quartering Seas ($\mu = 45^\circ$)	74
17.	Pitching Motion of Jackup Rig Prototype (Scale Ratio = 68.5). .	75

NOMENCLATURE

A_w	waterplane area
a	wave amplitude
B	beam or restoring coefficient
C	two-dimensional added mass coefficient
F	force or moment
G	center of gravity or source potential
g	gravitational constant
I	moment of inertia of the hull about an axis through the center of gravity
L	length of hull
l	hydrodynamic moment arm
M	moment or inertial coefficient
M''	three-dimensional added mass
m	number of mode or sectional mass
m''	two-dimensional added mass
N	two-dimensional or three-dimensional damping coefficient
O	origin of the coordinate system
p	hydrodynamic pressure
Q	source intensity
s	chord length
T	draft or period
t	time
U	amplitude of swaying velocity
V	amplitude of heaving velocity

W	weight
X,Y,Z	space coordinates
x,y,z	body coordinates

Subscripts

f	suffix designating force or moment
H	half beam-to-draft ratio, or indicating heave in two-dimensional hydrodynamics
h	wave elevation, or suffix designating wave
i	$\sqrt{-1}$, or suffix indicating the imaginary part or damping part
R	suffix indicating roll in two-dimensional hydrodynamics
r	suffix indicating the real part or inertial part
S	suffix in indicating swaying motion in two-dimensional hydrodynamics

Greek Letters

χ	yaw, or suffix designating yawing motion or yaw-exciting moment
Δ	displacement
δ	damping coefficient
ϵ	phase difference
η	sway, or suffix designating swaying motion or swaying-exciting force
κ	radius of gyration
Λ	tuning factor
λ	wavelength
μ	wave incidence
∇	volume displacement
ν	wave number

Ω	amplitude of rolling angular velocity in two-dimensional hydrodynamics
ω	circular frequency
ϕ	velocity potential
ψ	velocity potential or roll, or suffix designating rolling motion or roll-exciting moment
\downarrow	pitch, or suffix designating pitching motion or pitch-exciting moment
ρ	water density
ζ	heave, or suffix designating heaving motion or heave-exciting force

INTRODUCTION

During the past several years, a number of ocean platforms have failed structurally, and in many cases operations have had to be curtailed or delayed because of loads or motions induced by ocean waves. Now two years of study at Stevens Institute, sponsored by the Sea Grant Program of the National Science Foundation, have led to the development of reliable analytical techniques for studying platform motions during the design stage. In the future, additional realistic mechanisms affecting platform motions will be included in these analytical procedures so that a versatile, useful prediction capability can be attained.

It is hoped that the use of these methods, in conducting studies at the design stage, will make it possible to avoid operational delay and failure. The results of the design studies should, moreover, prove useful in evaluating the operational qualities of various designs, so that optimum performance can be achieved.

Ocean platforms can be classified, operationally, with respect to the effects induced by ocean waves. They fall into three main groups -- surface platforms, semi-submersible platforms, and bottom-supported platforms like the jackup drill rigs. This report is concerned with two subgroups of surface platforms whose hull shapes may be described as conventional ship forms or as barges. It should be noted that before emplacement many jackup rigs operate with a barge type of hull. Hence this kind of platform is included in the study.

The main target of this investigation is the determination of a reliable prediction method for surface platforms with conventional ship-type or barge-type hulls, operating in regular oblique seas. In future studies, procedures will be extended to the study of other hull types and other groups of platforms. The important motions of a platform in waves are coupled heaving, pitching, and surging; and coupled swaying, yawing, and rolling. The mean drifting motion and loads are also important wave effects which will be included in the future.

To solve for the coupled motions, we ought first to determine the forces and moments exerted on the platform oscillating in waves. Thus the first step in the investigation is to determine the hydrodynamic forces and moments exerted on a hull oscillating in calm water. The second step is to develop a prediction method for wave-exciting forces and moments on a restrained surface-type model in regular oblique seas. The third step is then to solve for the motions and to make comparisons with experimental results for confirmation of the prediction method.

In the present study, the first two steps make use of extensions of Frank's work¹ to the determination of the moment arms of the hydrodynamic forces exerted on a hull oscillating in a calm water surface, and to the calculation of wave-exciting forces and moments on a restrained hull in oblique regular seas. The third step involves a study of the hydrodynamic forces and moments and motions in connection with specific models and experimental data.

HYDRODYNAMIC FORCES AND MOMENTS ON CYLINDERS OSCILLATING IN CALM WATER

Frank¹ has reported on a method of calculating the hydrodynamic forces and moments for swaying, heaving, and rolling cylinders in and below the calm water surface. The method assumes a discrete distribution of two-dimensional pulsating sources on the submerged cylindrical contours, where the source intensities are determined by satisfying the kinematical boundary condition on the cylindrical surface.

The potential thus determined gives us the hydrodynamic pressure distribution on the cylindrical contour in the form .

$$p^{(m)} = p_r^{(m)} \cos \omega t + p_i^{(m)} \sin \omega t$$

where $m = 2, 3, 4$ (sway, heave, roll). The hydrodynamic forces and moments that are determined by integrating the pressure distribution consist of an inertial part, which is in phase with the acceleration of the oscillation, and a damping part, which is in phase with the velocity of the oscillation. The component forces and moments are formulated as shown below.

	Inertial Force	Damping Force
Vertical force due to heave	$F_{Hr} = \int_C p_r^{(3)} dy$	$F_{Hi} = \int_C p_i^{(3)} dy$
Lateral force due to sway	$F_{Sr} = \int_C - p_r^{(2)} dz$	$F_{Si} = \int_C - p_i^{(2)} dz$
Longitudinal rolling moment due to sway	$M_{Sr} = \int_C p_r^{(2)} (y dy + z dz)$	$M_{Si} = \int_C p_i^{(2)} (y dy + z dz)$
Lateral force due to roll	$F_{Rr} = \int_C - p_r^{(4)} dz$	$F_{Ri} = \int_C - p_i^{(4)} dz$
Longitudinal rolling moment due to roll	$M_{Rr} = \int_C p_r^{(4)} [y dy + (z - z_0) dz]$	$M_{Ri} = \int_C p_i^{(4)} [(y dy + (z - z_0) dz)]$

In these formulations , z_0 designates the coordinate of the center of rotation G in the z-axis, as shown in Fig. 1A. The moments M_{Sr} and M_{Si} are about the origin 0 , whereas M_{Rr} and M_{Ri} are about the center of gravity G . The forces and moments follow the sign convention of the right-handed coordinate system.

From the inertial and damping forces (moments), we define the added-mass coefficient, the added-moment-of-inertia coefficient, and the damping-force(moment) coefficient. These are represented in dimensionless form. In the case of sway and roll, it is necessary, in addition, to define the added moment arm and the damping moment arm which relate to the moment and force of the inertial and damping parts respectively. It is convenient to represent all these in the table shown below, where B = beam and T = draft.

	Heave	Sway	Roll
Inertial force	F_{Hr}	F_{Sr}	F_{Rr}
damping force	F_{Hi}	F_{Si}	F_{Ri}
Inertial moment		M_{Sr}	M_{Rr}
damping moment		M_{Si}	M_{Ri}
added mass	$m_H'' = \frac{F_{Hr}}{\omega V}$	$m_S'' = \frac{F_{Sr}}{\omega U}$	$m_R'' = \frac{M_{Rr}}{\omega \Omega}$
added moment of inertia			
damping force coefficient	$N_H = \frac{F_{Hi}}{V}$	$N_S = \frac{F_{Si}}{U}$	
damping moment coefficient			$N_R = \frac{M_{Ri}}{\Omega}$
added-mass coefficient	$C_H = \frac{m_H''}{\rho \frac{\pi}{8} B^2}$	$C_S = \frac{m_S''}{\rho \frac{\pi}{2} T^2}$	$C_R = \frac{m_R''}{\rho \frac{\pi}{8} T^4}$
added-moment-of-inertia coefficient			
damping force parameter	$\delta_H = \frac{N_H}{\rho \omega \frac{\pi}{8} B^2}$	$\delta_S = \frac{N_S}{\rho \omega \frac{\pi}{2} T^2}$	$\delta_R = \frac{N_R}{\rho \omega \frac{\pi}{8} T^4}$
damping moment parameter			
added moment arm		$\frac{l_{Sr}}{T} = \frac{M_{Sr}}{F_{Sr} T}$	$\frac{l_{Rr}}{T} = \frac{M_{Rr}}{F_{Rr} T}$
damping moment arm		$\frac{l_{Si}}{T} = \frac{M_{Si}}{F_{Si} T}$	$\frac{l_{Ri}}{T} = \frac{M_{Ri}}{F_{Si} T}$

In the table on the previous page , V , U , and Ω designate, respectively, the heave velocity amplitude, the sway velocity amplitude, and the roll angular velocity amplitude. The moment arm induced by rolling motion is taken from the center of rotation. The moment arms induced both by roll (l_{Rr} , l_{Ri}) and by sway (l_{Sr} , l_{Si}) indicate the positions of the lateral forces applied, these are positive if the applied force is below the center of rotation G in the case of roll, or below the origin of the coordinate O for swaying motion.

The hydrodynamic forces and moments thus obtained are two-dimensional. The strip method serves as a bridge in extending two-dimensional calculation to calculation for the three-dimensional platform configurations.

WAVE-EXCITING FORCES AND MOMENTS ON A RESTRAINED BODY IN OBLIQUE SEAS

Grim's two-dimensional method^{2,3} is based on the assumption that the disturbance of an incident wave caused by the ship's body is represented by the potential used in describing the water flow around the body, when the body is oscillating harmonically in the calm water surface. This potential, together with the incident wave potential, constitutes the potential that describes the flow around the body under restraint in waves.

In the present study, we select, for the disturbance, the potential used by Frank¹. His method enables us to compute hydrodynamic forces and moments not only for the non-Lewis cylindrical form but also for the widely varying configurations of ocean platforms of the semi-submersible type.

In order to introduce the strip method by Grim⁴ we first define the coordinate system and incident waves.

Let $O-XYZ$ and $O-xyz$ be the right-handed rectangular coordinate systems, as illustrated in Fig. 1B. Coordinate planes $O-XY$ and $O-xy$ lie on the calm water surface, and the Z - and z -axes point vertically upward. The center of gravity of the body, G , lies on the z -axis. Let the incident wave heading be designated by μ and let the wave progress in the positive Y -direction. Then the wave profile is

$$h = a \cos (\nu Y - \omega t)$$

In the space coordinates, and

$$h = a \cos (\nu y \sin \mu + \nu x \cos \mu - \omega t) \quad (2.1)$$

In the body coordinates, where

a = wave amplitude

ν = wave number (ω^2/g)

ω = circular wave frequency

Now, suppose two vertical control planes cut the body at x and $x + dx$; and consider the wave motion within the fictitiously confined domain. The wave equation (2.1) can be interpreted by noting that the term $v_y \sin \mu$ determines the wave form in the two-dimensional domain, and that the term $v_x \cos \mu$ represents the phase shift of the wave between locations $x = 0$ and $x = x$. Cutting the whole body by many vertical control planes such as are demonstrated above, we can apply the strip method, or the cross-flow hypothesis, in each plane. That is, the three-dimensional forces on the restrained body, induced by the oblique waves, can be determined approximately by summation of the two-dimensional elementary forces induced by the waves on each strip.

The potential of the wave Eq.(2.1) is represented by

$$\varphi = \frac{ga}{\omega} e^{vz} \sin (v_y \sin \mu + v_x \cos \mu - \omega t)$$

or, conveniently, by the wave potential per unit amplitude of the incident wave

$$\frac{1}{a} \varphi(x, y, z ; t, \mu) = \frac{g}{\omega} e^{vz} \sin (v_y \sin \mu + v_x \cos \mu - \omega t) \quad (2.2)$$

The terms $v_y \sin \mu$ and $v_x \cos \mu$ have physical meanings interpreted as aforementioned.

The wave potential is broken down into two component potentials, of the form

$$\frac{1}{a} \varphi_o = \frac{g}{\omega} e^{vz} \sin (v_y \sin \mu) \cdot \cos (v_x \cos \mu - \omega t) \quad (2.3)$$

$$\frac{1}{a} \varphi_e = \frac{g}{\omega} e^{vz} \cos (v_y \sin \mu) \cdot \sin (v_x \cos \mu - \omega t) \quad (2.4)$$

Since the potentials $\frac{1}{a} \varphi_o$ and $\frac{1}{a} \varphi_e$ are, respectively, the odd and even functions of y , the odd function $\frac{1}{a} \varphi_o$ is applied to the asymmetric motion of water about the z -axis in the yz -plane, and the even function,

$\frac{1}{a} \varphi_e$, is applied to the symmetric motion of water about the z-axis.

Therefore the odd function will be employed as the potential causing the sway force and roll moment on a cylinder section in the beam sea, and the even one will be used as the potential causing the heave force on the section.

The disturbance potential must be added to the wave potential derived above, to account for the actual presence of the body. The disturbance is mathematically expressed by a distribution of pulsating sources over the two-dimensional section surface. The potential used by Frank¹ is employed as our disturbance potential. Since the disturbance depends on the incident wave and on the position and form of the body sections, it can be written

$$\Phi^{(m)}(x, y, z; \mu, t) = \operatorname{Re} \left[\int_C Q^{(m)}(s) \cdot G(y, z; \eta, \zeta) e^{i(\nu x \cos \mu - \omega t)} ds \right] \quad (2.5)$$

In this equation, m designates the mode of excitation ($m=2, 3, 4$ = sway, heave, roll), and the expression $Q^{(m)}(s)$ designates the unknown complex source intensities distributed along the section contour C . The expression depends on the mode of excitation, the geometry of the section, and the incident wave. The expression $G(y, z; \eta, \zeta)$ is the pulsating source potential of unit intensity at the point (η, ζ) in the lower-half yz -plane of Fig. 1A. The term $e^{i\nu x \cos \mu}$ in Eq. (2.5) represents the phase shift due to the position of the section x where the disturbance occurs in response to the oblique incident wave of wave number ν and incidence μ .

Since $Q^{(m)}$ and G are the complex source intensity and source function, respectively, let them be denoted as

$$Q^{(m)} = Q_r^{(m)} + iQ_i^{(m)}$$

$$G = G_r + i(-G_i)$$

where $i = \sqrt{-1}$, and where $Q_r^{(m)}$ and $Q_i^{(m)}$ are real and imaginary parts of $Q^{(m)}$, and G_r and $-G_i$ are real and imaginary parts of G .

Equation (2.5) is then changed to

$$\begin{aligned} \bar{\phi}^{(m)} &= \int_C (Q_r^{(m)} G_r + Q_i^{(m)} G_i) ds \\ &\cdot \cos (vx \cos \mu - \omega t) \\ &- \int_C (-Q_r^{(m)} G_i + Q_i^{(m)} G_r) ds \\ &\cdot \sin (vx \cos \mu - \omega t) \end{aligned} \tag{2.6}$$

The ultimately required potential which describes the water flow around the restrained body in the strip region is therefore obtained by superimposing the wave potential (2.2) and the corresponding disturbance potential (2.6). Specifically, the potentials are written according to the mode of excitation (i.e., sway, heave, and roll), as

$$\begin{aligned} \bar{\phi}_S &= \bar{\phi}^{(2)} + \frac{1}{a} \varphi_o \\ \bar{\phi}_H &= \bar{\phi}^{(3)} + \frac{1}{a} \varphi_e \\ \bar{\phi}_R &= \bar{\phi}^{(4)} + \frac{1}{a} \varphi_o \end{aligned} \tag{2.7}$$

The potentials $\bar{\phi}_H$, $\bar{\phi}_S$, and $\bar{\phi}_R$ satisfy the following four conditions, out of the five required⁶

- (1) The continuity of the liquid in the whole domain
- (2) The linearized free-surface condition
- (3) The radiation condition
- (4) The deepwater condition

The fifth condition to be satisfied is the kinematical boundary condition on the body surface (no flow through the surface of the restrained body). For

the three modes of excitation, we write

$$\frac{\partial}{\partial n}(\Phi_H) = 0 ; \frac{\partial}{\partial n}(\Phi_S) = 0 ; \frac{\partial}{\partial n}(\Phi_R) = 0 \quad (2.8)$$

By solving Eq. (2.8), we determine the unknown source intensities; and thence linear hydrodynamic pressures induced at a point on the body surface by the incident wave of unit amplitude are obtained from

$$\frac{a}{p_S} = - p \frac{\partial \Phi_S}{\partial t} \quad (\text{for sway})$$

$$\frac{a}{p_H} = - p \frac{\partial \Phi_H}{\partial t} \quad (\text{for heave})$$

$$\frac{a}{p_R} = - p \frac{\partial \Phi_R}{\partial t} \quad (\text{for roll})$$

(2.9)

The integration of these pressures over the submerged surface of the body gives the wave-exciting forces and moments on the body per unit amplitude of the incident wave. The following symbols are introduced for the forces and moments

F_ξ surge-exciting force

F_η sway-exciting force

F_ζ heave-exciting force

F_ϕ roll-exciting moment about G

F_ψ pitch-exciting moment about G

F_χ yaw-exciting moment about G

They are represented in the formulas which follow on page 12.

$$\begin{aligned} \frac{F_G}{a} &= \int_L \int_C \frac{P_H}{a} dy dx = \frac{F_{Gr}}{a} \cos \omega t + \frac{F_{Gi}}{a} \sin \omega t \\ &= \sqrt{\left(\frac{F_{Gr}}{a}\right)^2 + \left(\frac{F_{Gi}}{a}\right)^2} \cos(\omega t + \epsilon_{fGh}) \end{aligned}$$

with
$$\epsilon_{fGh} = \tan^{-1} \frac{-F_{Gi}}{F_{Gr}} ;$$

$$\begin{aligned} \frac{F_\eta}{a} &= \int_L \int_C -\frac{P_S}{a} dz dx = \frac{F_{\eta r}}{a} \cos \omega t + \frac{F_{\eta i}}{a} \sin \omega t \\ &= \sqrt{\left(\frac{F_{\eta r}}{a}\right)^2 + \left(\frac{F_{\eta i}}{a}\right)^2} \cos(\omega t + \epsilon_{f\eta h}) \end{aligned}$$

with
$$\epsilon_{f\eta h} = \tan^{-1} \frac{-F_{\eta i}}{F_{\eta r}} ;$$

$$\begin{aligned} \frac{F_X}{a} &= \int_L \int_C -\frac{P_S}{a} x dz dx = \frac{F_{Xr}}{a} \cos \omega t + \frac{F_{Xi}}{a} \sin \omega t \\ &= \sqrt{\left(\frac{F_{Xr}}{a}\right)^2 + \left(\frac{F_{Xi}}{a}\right)^2} \cos(\omega t + \epsilon_{fXh}) \end{aligned}$$

with
$$\epsilon_{fXh} = \tan^{-1} \frac{-F_{Xi}}{F_{Xr}} ;$$

$$\begin{aligned} \frac{F_{\psi}}{a} &= \int_L \int_C -\frac{P_H}{a} x \, dy \, dx = \frac{F_{\psi r}}{a} \cos \omega t + \frac{F_{\psi i}}{a} \sin \omega t \\ &= \sqrt{\left(\frac{F_{\psi r}}{a}\right)^2 + \left(\frac{F_{\psi i}}{a}\right)^2} \cos(\omega t + \epsilon_{f\psi h}) \end{aligned}$$

with
$$\epsilon_{f\psi h} = \tan^{-1} \frac{-F_{\psi i}}{F_{\psi r}} ;$$

$$\begin{aligned} \frac{F_{\varphi}}{a} &= \int_L \int_C \frac{P_R}{a} [y \, dy + (z-z_0) \, dz] \, dx = \frac{F_{\varphi r}}{a} \cos \omega t + \frac{F_{\varphi i}}{a} \sin \omega t \\ &= \sqrt{\left(\frac{F_{\varphi r}}{a}\right)^2 + \left(\frac{F_{\varphi i}}{a}\right)^2} \cos(\omega t + \epsilon_{f\varphi h}) \end{aligned}$$

with
$$\epsilon_{f\varphi h} = \tan^{-1} \frac{-F_{\varphi i}}{F_{\varphi r}}$$

(2.10)

where L means that the integration is executed over the length of the body, C means integration over the contour of a section, and ϵ designates the phase difference between the wave maximum at the origin and the force or moment maximum. Positive ϵ indicates phase lead of the force from the wave. The surge-exciting force $\frac{F_{\xi}}{a}$, may if the restrained body is geometrically symmetrical about the y-axis, be calculated by taking the strip in the direction parallel to the x-axis. The positive signs of the forces and moments take the positive directions of the right-handed coordinate system as shown in Fig. 1C.

The numerically calculated examples and the comparison with the experimental results were reported earlier.⁶ The reliability of the present prediction method was confirmed.

COUPLED EQUATIONS OF MOTION IN OBLIQUE SEAS

The coupled heaving and pitching motions and the coupled swaying, yawing, and rolling motions are considered. The right-handed coordinate system is shown in Fig. 1C. The body coordinate system is designated by 0-xyz. In this system, the 0-xy plane lies on the calm water surface and the z-axis passes through the center of gravity G. The oscillatory motions are about the center of gravity G as shown in Fig. 1C.

COUPLED HEAVING AND PITCHING EQUATIONS

The heaving and pitching equations are written as^{7,8}

$$\begin{aligned}
 & (-\omega^2 M_{\zeta\zeta} + i\omega N_{\zeta\zeta} + B_{\zeta\zeta}) \bar{\zeta}(\omega) - (-\omega^2 M_{\psi\zeta} + i\omega N_{\psi\zeta} + B_{\psi\zeta}) \bar{\psi}(\omega) \\
 & \qquad \qquad \qquad = F_{\zeta r} - i F_{\zeta i} \\
 & - (-\omega^2 M_{\zeta\psi} + i\omega N_{\zeta\psi} + B_{\zeta\psi}) \bar{\zeta}(\omega) + (-\omega^2 M_{\psi\psi} + i\omega N_{\psi\psi} + B_{\psi\psi}) \bar{\psi}(\omega) \\
 & \qquad \qquad \qquad = F_{\psi r} - i F_{\psi i} \\
 & \qquad \qquad \qquad (3.1)
 \end{aligned}$$

The heave-exciting and pitch-exciting force and moment are obtained from Eq. (2.10). The symbols $\bar{\zeta}(\omega)$ and $\bar{\psi}(\omega)$ are the Fourier transforms of $\zeta(t)$ and $\psi(t)$ the heave and pitch motions, respectively, with the expressions

$$\bar{\zeta} = \zeta_r + i\zeta_i \quad \text{and} \quad \bar{\psi} = \psi_r + i\psi_i$$

and

$$\epsilon_{\zeta h} = \tan^{-1} \frac{\zeta_i}{\zeta_r} \quad \text{and} \quad \epsilon_{\psi h} = \tan^{-1} \frac{\psi_i}{\psi_r}$$

The positive ϵ 's mean that the phase of the motion maximum leads the wave maximum at the origin.

The coefficients in the left-hand side are defined by the formulas

$$M_{\zeta\zeta} = \int_{-l_1}^{l_2} (m+m_H'') dx = \rho\nabla + \int_{-l_1}^{l_2} m_H'' dx$$

$$N_{\zeta\zeta} = \int_{-l_1}^{l_2} N_H dx$$

$$B_{\zeta\zeta} = \rho g \int_{-l_1}^{l_2} 2 y_w dx = \rho g A_w$$

$$M_{\psi\zeta} = M_{\zeta\psi} = \int_{-l_1}^{l_2} m_H'' x dx$$

$$N_{\psi\zeta} = N_{\zeta\psi} = \int_{-l_1}^{l_2} N_H x dx$$

$$B_{\psi\zeta} = B_{\zeta\psi} = \rho g \int_{-l_1}^{l_2} 2 y_w x dx$$

$$M_{\psi\psi} = I_{\psi} + \int_{-l_1}^{l_2} m_H'' x^2 dx$$

$$N_{\psi\psi} = \int_{-l_1}^{l_2} N_H x^2 dx$$

$$B_{\psi\psi} = \rho g \int_{-l_1}^{l_2} 2 y_w x^2 dx = \rho g \nabla \overline{GM}_{\psi}$$

where

m = sectional mass of the hull

∇ = total volume of the immersed hull

A_w = waterplane area

y_w = half-beam of a section in the waterplane

\overline{GM}_{ψ} = longitudinal metacentric height

I_{ψ} = longitudinal moment of inertia of the hull about the transverse axis through G

The two-dimensional added mass and damping force coefficient for heaving (i.e., m_H'' and N_H) are determined by the method described in the first section of this report.

Equations (3.1) are reduced to the matrix equation

$$\begin{bmatrix} \left\{ (B_{\zeta\zeta} - \omega^2 M_{\zeta\zeta}) + i\omega N_{\zeta\zeta} \right\} & - \left\{ (B_{\psi\zeta} - \omega^2 M_{\psi\zeta}) + i\omega N_{\psi\zeta} \right\} \\ - \left\{ (B_{\psi\zeta} - \omega^2 M_{\psi\zeta}) + i\omega N_{\psi\zeta} \right\} & \left\{ (B_{\psi\psi} - \omega^2 M_{\psi\psi}) + i\omega N_{\psi\psi} \right\} \end{bmatrix} \begin{bmatrix} \bar{\zeta}/a \\ \bar{\psi}/a \end{bmatrix} = \begin{bmatrix} \bar{F}_\zeta/a \\ \bar{F}_\psi/a \end{bmatrix}$$

$$\bar{F}_\zeta = F_{\zeta r} + i (-F_{\zeta i})$$

$$\bar{F}_\psi = F_{\psi r} + i (-F_{\psi i})$$

(3.2)

Solving for the motions $\bar{\zeta}/a$ and $\bar{\psi}/a$, we determine the dimensionless motion parameters $\bar{\zeta}/a$ and $\bar{\psi}/a$ which give us the amplitude of the motion and the phase difference between the wave maximum at the origin 0 and the motion maximum.

COUPLED SWAYING, YAWING, AND ROLLING EQUATIONS

To derive coupled swaying, yawing, and rolling equations, which will be consistent with our coordinate system, we consider the dynamic equilibrium equations for each mode of motion.^{4,7} Taking a form similar to Eqs. (3.1), these equations of motion in the frequency plane are written

$$(-\omega^2 M_{\eta\eta} + i\omega N_{\eta\eta}) \bar{\eta}(\omega) + (-\omega^2 M_{\chi\eta} + i\omega N_{\chi\eta}) \bar{\chi}(\omega) + (-\omega^2 M_{\varphi\eta} + i\omega N_{\varphi\eta}) \bar{\varphi}(\omega) = \bar{F}_\eta$$

$$(-\omega^2 M_{\eta\chi} + i\omega N_{\eta\chi}) \bar{\eta}(\omega) + (-\omega^2 M_{\chi\chi} + i\omega N_{\chi\chi}) \bar{\chi}(\omega) + (-\omega^2 M_{\varphi\chi} + i\omega N_{\varphi\chi}) \bar{\varphi}(\omega) = \bar{F}_\chi$$

$$(-\omega^2 M_{\eta\varphi} + i\omega N_{\eta\varphi}) \bar{\eta}(\omega) + (-\omega^2 M_{\chi\varphi} + i\omega N_{\chi\varphi}) \bar{\chi}(\omega) + (-\omega^2 M_{\varphi\varphi} + i\omega N_{\varphi\varphi} + B_{\varphi\varphi}) \bar{\varphi}(\omega) = \bar{F}_\varphi$$

(3.3)

where the complex exciting forces and moments on the right-hand side are determined from Eq. (2.10) in the expressions

$$\bar{F}_\eta = F_{\eta r} + i(-F_{\eta i}) ; \bar{F}_\chi = F_{\chi r} + i(-F_{\chi i}) ;$$

$$\bar{F}_\varphi = F_{\varphi r} + i(-F_{\varphi i})$$

and the complex motions are written in the forms

$$\bar{\eta} = \eta_r + i\eta_i ; \bar{\chi} = \chi_r + i\chi_i ; \bar{\varphi} = \varphi_r + i\varphi_i$$

with

$$\epsilon_{\eta h} = \tan^{-1} \frac{\eta_i}{\eta_r}$$

$$\epsilon_{\chi h} = \tan^{-1} \frac{\chi_i}{\chi_r}$$

$$\epsilon_{\varphi h} = \tan^{-1} \frac{\varphi_i}{\varphi_r}$$

The positive ϵ 's mean that the phase of the motion maximum leads the wave maximum at the origin.

The coefficients in the left-hand side of Eq. (3.3) are determined by the formulas; that is,

$$M_{\eta\eta} = \int_{-l_1}^{l_2} (m+m_S'') dx = \rho V + \int_{-l_1}^{l_2} m_S'' dx$$

$$N_{\eta\eta} = \int_{-l_1}^{l_2} N_S dx$$

$$M_{\chi\eta} = M_{\eta\chi} = \int_{-l_1}^{l_2} m_S'' x dx$$

$$N_{\chi\eta} = N_{\eta\chi} = \int_{-l_1}^{l_2} N_S x dx$$

$$M_{\varphi\eta} = \int_{-l_1}^{l_2} \frac{m_R''}{l_{Rr}} dx$$

$$N_{\varphi\eta} = \int_{-l_1}^{l_2} \frac{N_R}{l_{Ri}} dx$$

$$M_{\chi\chi} = I_{\chi} + \int_{-l_1}^{l_2} m_S'' x^2 dx$$

$$N_{\chi\chi} = \int_{-l_1}^{l_2} N_S x^2 dx$$

$$M_{\varphi\chi} = \int_{-l_1}^{l_2} \frac{m_R''}{l_{Rr}} x dx$$

$$N_{\varphi\chi} = \int_{-l_1}^{l_2} \frac{N_R}{l_{Ri}} x dx$$

$$M_{\eta\varphi} = \int_{-l_1}^{l_2} m_S'' (\pm \overline{OG} + l_{Sr}) dx$$

$$N_{\eta\varphi} = \int_{-l_1}^{l_2} N_S (\pm \overline{OG} + l_{Si}) dx$$

$$M_{\chi\varphi} = \int_{-l_1}^{l_2} m_S'' (\pm \overline{OG} + l_{Sr}) dx$$

$$N_{\chi\varphi} = \int_{-l_1}^{l_2} N_S (\pm \overline{OG} + l_{Si}) x dx$$

$$M_{\varphi\varphi} = I_{\varphi} + \int_{-l_1}^{l_2} m_R'' dx$$

$$N_{\varphi\varphi} = \int_{-l_1}^{l_2} N_R dx$$

$$B_{\varphi\varphi} = \rho g \nabla \overline{GM}_{\varphi}$$

where

$\rho \nabla =$ total mass of the ship

$\pm \overline{OG}$ = distance between the origin and the center of gravity G. The + sign is taken for G above O, and the - sign is taken for G below O.

GM_{φ} = metacentric height for roll.

I_{χ} = moment of inertia of the ship about the vertical axis through G

I_{φ} = moment of inertia of the ship about the longitudinal axis through G

The above coefficients are easily calculated by the two-dimensional added mass and damping coefficients, etc., described in the first section.

Equations (3.3) are reduced to the following matrix equation:

$$\begin{bmatrix} (-\omega^2 M_{\eta\eta} + i\omega N_{\eta\eta}) & (-\omega^2 M_{\chi\eta} + i\omega N_{\chi\eta}) & (-\omega^2 M_{\varphi\eta} + i\omega N_{\varphi\eta}) \\ (-\omega^2 M_{\eta\chi} + i\omega N_{\eta\chi}) & (-\omega^2 M_{\chi\chi} + i\omega N_{\chi\chi}) & (-\omega^2 M_{\varphi\chi} + i\omega N_{\varphi\chi}) \\ (-\omega^2 M_{\eta\varphi} + i\omega N_{\eta\varphi}) & (-\omega^2 M_{\chi\varphi} + i\omega N_{\chi\varphi}) & (B_{\varphi\varphi} - \omega^2 M_{\varphi\varphi} + i\omega N_{\varphi\varphi}) \end{bmatrix} \begin{bmatrix} \frac{\overline{\eta}}{a} \\ \frac{\overline{\chi}}{a} \\ \frac{\overline{\varphi}}{a} \end{bmatrix} = \begin{bmatrix} \frac{\overline{F}_{\eta}}{a} \\ \frac{\overline{F}_{\chi}}{a} \\ \frac{\overline{F}_{\varphi}}{a} \end{bmatrix} \quad (3.4)$$

From the solution of Eq. (3.4), we obtain the dimensionless parameters for sway, yaw, and roll; that is,

$$\frac{\overline{\eta}}{a}, \quad \frac{\overline{\chi}}{va}, \quad \text{and} \quad \frac{\overline{\varphi}}{va}$$

MOTION OF A SHIP-SHAPED PLATFORM IN OBLIQUE SEAS

MODEL AND MODEL TEST CONDITION

We consider the motion of the Series 60 ship model⁷ in oblique seas. Tasai reported on the vertical and lateral coupled motions of the Series 60 model in beam seas. This model is an appropriate one for our investigation, since it has been studied theoretically as well as experimentally. The principal particulars and the test conditions are shown in the tables below.

MODEL PARTICULARS

$L_{BP} = 3.0$ m	$C_B = 0.70$
$B = 0.428$ m	$C_p = 0.710$
$L/B = 7.0$	$C_{\phi} = 0.985$
$D = 0.267$ m	$C_w = 0.785$
$T = 0.171$ m	$\phi_B = 0.013$ m fore
$W = \rho g \nabla = 153.74$ kg	$KB = 9.02$ cm

(Radius of gyration of pitching in air $r_{\psi} = 0.24 L_{BP}$ even keel; without bilge keel and propeller; with rudder.)

TEST CONDITION

$\overline{GM}_{\phi} = 2.78$ cm	$KG = 14.66$ cm
$\delta_1 = 0.0770$	$\delta_2 = 0.0044$ (1/deg)
$\phi_B = 0.0314$ m aft, even keel	$T = 0.171$ m
$\overline{OG} = 0.0244$ m	
Natural rolling period $T_{\phi} = 1.61$ sec	
Natural pitching period $T_{\psi} = 1.00$ sec	
Natural heaving period $T_{\zeta} = 1.03$ sec	

In the strip calculation described in the previous sections, thirteen transverse strips were taken (i.e., the following station numbers: 0, 1, 2, 4, 6, 8, 10, 12, 14, 16, 18, 19, and 20). For the calculation of two-dimensional hydrodynamic forces and moments on each strip, eleven source points were taken for heaving and swaying motions while 20 source points were used for rolling motions.

In the following discussion, we consider first the calculated results for vertical plane motions, then the lateral coupled motions.

COUPLED HEAVING AND PITCHING MOTIONS

We refer to the vertical coupled motions, Eq. (3.1). The heave and pitch inertial and damping coefficients are plotted against the frequency parameter \sqrt{T} in Fig. 2; and the heave- and pitch-exciting forces and moments on the ship model are plotted in Fig. 3 as functions of wave-to-ship length ratio λ/L in beam seas ($\mu = 90^\circ$). Both heave and pitch inertial coefficients and both heave and pitch damping coefficients have the same trends in Fig. 2. The response motions in heave and pitch are illustrated as functions of wave-to-ship length ratio in Figs. 4A and 4B. The peaks of both motions occur at their natural periods. The predictions are seen to be in good agreement with the experimental results.⁷

Next we examine the coupled motions of the ship model in oblique seas, with wavelength to ship length ratios 0.5, 1.0 and 2.0. The heave- and pitch-exciting forces and moments are shown in Figs. 5A and 5B as functions of incidence μ and wavelength to ship length ratio λ/L . In general, the heaving-force maxima occur in beam seas. The maximum force in the beam seas increases as the wavelength increases. On the contrary, pitching-moment minima generally occur in beam seas. The location of the incidence μ where the maximum moment occurs moves toward head sea or following sea 180° or 0° as the wavelength to ship length ratio increases (Fig. 5B). Referring to Figs. 6A and 6B, we consider the heave and pitch responses as functions of λ/L and μ . Since the heaving and pitching natural periods are coincident with the wave periods of $\lambda/L = 0.55$ and 0.52 , respectively, we may, for explanatory purpose, take the heave and pitch curves for

$\lambda/L = 0.5$ roughly as the resonant heaving and pitching motions. By this assumption, the resonant heave and pitch are reduced to the functions of the incidence μ only. The maximum of the resonant heaving motion occurs in the beam seas, while the maximum of the resonant pitching motion occurs in the quartering seas.

The heave motion is greatest at the resonant condition, but this is not necessarily true of pitch motion.

COUPLED SWAYING, YAWING, AND ROLLING MOTIONS

Referring to the lateral coupled equation (3.3), we observe the calculated results of the inertial and damping coefficients which are defined in the Appendix, as functions of frequency parameter νT in Figs. 7A, 7B, and 7C. The swaying and yawing inertial coefficients and the swaying and yawing damping coefficients behave in a similar manner as functions of the frequency, as should be expected (Fig. 7A). The rolling inertial coefficient is practically constant over the frequency range. In determining

$$I_{\varphi} = M_{\varphi\varphi} - \int_{-l_1}^{l_2} m_R'' dx$$

an approximation for $M_{\varphi\varphi}$ was obtained from the relation $T_{\varphi} \approx 2\pi \sqrt{\frac{M_{\varphi\varphi}}{B_{\varphi\varphi}}}$ (Fig. 7B).

Thus far, each hydrodynamic force component has been adequately described by means of linear inviscid theoretical analysis. In the case of roll motion, these assumptions have not been found adequate for predicting damping moments of conventional ship forms.⁷ For roll motions, Tasai has shown that a reliable description of the roll damping moment is given by

$$N_{\varphi\varphi}^* = \frac{M_{\varphi\varphi}}{\pi} \omega_{\varphi} (\delta_1 + \delta_2 \Lambda_{\varphi} |\bar{\varphi}|)$$

where

$\delta_1, \delta_2 =$ coefficients determined from the analysis of roll extinction curves (see page 21)

ω_φ = natural rolling frequency

$\Lambda_\varphi = \omega_w / \omega_\varphi$; ω_w = wave frequency

$|\bar{\varphi}|$ = roll motion amplitude

The linear damping moment due to wave-making only is compared in Fig. 7B with that predicted by this non-linear representation. Roll damping due to wave-making is apparently much less than that due to linear and non-linear viscous effects, for conventional ship forms. The coupled inertial and damping coefficients between roll and sway and between roll and yaw are illustrated in Fig. 7C. The roll \rightarrow sway coupled coefficients are not identical with the sway \rightarrow roll coupled coefficients; nor are the coupled coefficients from roll to yaw and yaw to roll identical. However, they have the same trend.

As the second step in the discussion of Eq. (3.3), we next consider the sway-, yaw-, and roll-exciting forces and moments plotted against the wave-to-ship length ratio λ/L in beam seas ($\mu = 90^\circ$). In Figs. 8A and 8B, it is seen that both the sway force and the roll moment approach asymptotes as wavelength λ increases, while yaw moment approaches its minimum limit. The sway force and roll moment decrease as the wave frequency increases. Contrary to this, the yawing moment increases as the frequency increases.

When non-linear roll damping moments are included, the solution of Eqs. (3.4) is not quite so simple as for the linear case. Replacing $N_{\varphi\varphi}$ with $N_{\varphi\varphi}^*$ given by

$$N_{\varphi\varphi}^* = \frac{M_{\varphi\varphi}}{\pi} \omega_\varphi (\delta_1 + \nu_a \delta_2 \Lambda_\varphi \frac{|\bar{\varphi}|}{\nu_a})$$

then equations (3.4) can be solved by iteration methods for $\frac{\bar{\eta}}{a}$, $\frac{\bar{\chi}}{\nu_a}$, and $\frac{\bar{\varphi}}{\nu_a}$ as a function of λ/L or equivalently, Λ_φ . However, the solution depends on the value of ν_a used in the expression for $N_{\varphi\varphi}^*$. First, the value $\nu_a = \pi/52.5$ was used, which is the mean of the wave characteristics for which the motions were measured.⁷

Having solved for the coupled motions (3.4) by applying the above information, we represent swaying motion as a function of wave period, T_w , yawing motion as a function of wavelength-to-ship length ratio, λ/L , and the rolling motion as a function of its tuning factor, Λ_ϕ , in Figs. 9A, 9B, and 9C.

The swaying amplitude is compared with the experimental results.⁷ The humps of both swaying amplitude and phase angle are ascribed to the coupled effect.⁷ The yawing motion, $\frac{|\bar{x}|}{v_a}$, also fluctuates near the natural rolling period. To understand the coupling effect, we compare the yawing motion with the uncoupled effect as shown in Fig. 9B.

In general, the yawing motion is negligibly small in comparison with the other two motions in beam seas. The calculation, however, reveals that the yaw amplitude ratio $\frac{|\bar{x}|}{v_a}$ increases as the wavelength λ/L increases above the natural roll period. This phenomenon must be checked experimentally.

Rolling motion is also in good agreement with the experimental results⁷ as shown in Fig. 9C. We should recall the introduction of the non-linear damping coefficient with $v_a = \pi/52.5$ there in the solution of Eq. (3.4).

Finally, the effect of the wave slope v_a on the rolling motions in beam seas ($\mu = 90^\circ$) were investigated; the coupled Eqs. (3.4) were solved for different given wave slopes (see Fig. 9D). It is seen from the figure that the wave slope has a large influence on the rolling motion prediction near resonance.

So far, we have discussed the motions of the ship model in beam seas ($\mu = 90^\circ$). We come now to the lateral coupled motion of the ship model in oblique seas with wavelength to ship length ratio $\lambda/L = 0.5, 1.35$ and 2.0 , and with the wave slope $v_a = \pi/52.5$. The period of the wave $\lambda/L = 1.35$ is coincident with the natural rolling period.

The sway-, yaw-, and roll-exciting forces and moments are shown in Figs. 10A, 10B and 10C as functions of incidence μ and wavelength λ/L . Similarly, the response motions sway, yaw, and roll are illustrated in Figs. 11A, 11B, and 11C as functions of μ and λ/L .

The sway-exciting force maxima occur in beam seas and increase as the wavelength becomes longer.

The yaw-exciting moment maxima generally occur in quartering seas, while the minima occur in beam seas. The roll-exciting moment maxima also occur generally in quartering seas and the number of fluctuations of the moment curves diminishes as the wavelength increases.

All the lateral exciting forces and moments vanish in head and in following seas.

The sway and yaw response motions in Figs. 11A and 11B have similar trends as the corresponding wave exciting force and moment.

The roll response curves are flattened out in comparison with the wave-exciting moment (Fig. 11C). It is seen from the figure that the resonant roll motion ($\lambda/L = 1.35$) is predominantly higher than the other motions ($\lambda/L = 0.5, 2.0$) although the roll-exciting moments for $\lambda/L = 1.35$ and 2.0 are, in effect, not different at all. This explains the characteristic behavior of a ship's roll in irregular waves. In other words, the spectral energy of the roll response motion is mostly distributed in a narrow wave frequency band in the neighborhood of the roll natural frequency.

MOTION OF JACKUP RIG MODEL IN OBLIQUE SEAS

MODEL AND MODEL TEST CONDITIONS

We consider the vertical and lateral coupled motions of a jackup rig model in oblique seas. The jackup rig model used in our investigation was selected because it was representative of recently constructed drill-rig ocean platforms. The principal particulars and the tested conditions are given in the tables below.

MODEL PARTICULARS

Length , L	30.7 in.
Beam , B	20.45 in.
Depth , D	2.98 in.
Draft , T	1.93 in.
Displacement , Δ	43.60 lb

Hull

Weight , W	34.4 lb
LCG	Ø
VCG, above waterline	3.24 in.
Pitch gyradius	8.76 in.
Roll gyradius	6.31 in.

(Section forms: same rectangular section used throughout.)

Legs

Length	43.8 in.
Total weight	9.12 lb
Weight/ft	0.642 lb/ft
Diameter	1.75 in.

TEST CONDITIONS

Legs Up

Natural pitching period	1.085 sec
Natural heaving period	0.905 sec
Logarithmic decrement for pitch	$\delta_1 = 0.566$

Legs Half Down

Natural pitching period	1.014 sec
Natural rolling period	1.123 sec
Natural heaving period	0.966 sec

Legs Full Down

Natural pitching period	1.328 sec
Natural rolling period	1.654 sec
Natural heaving period	1.002 sec

TEST PROCEDURE

The heaving and pitching motions of the jackup rig model in head seas were measured in Tank No. 2 at Davidson Laboratory. The motions of the model with its legs up, half down, and full down were investigated. The motions of the model with the legs in waves simulate various operational stages of a drill-rig platform in waves before and while the legs are lowered at an oil-drilling location. Photographs of the model are shown in Fig. 12.

HEAVING, PITCHING, AND SURGING MOTIONS

We consider only the motion of the jackup rig model with legs up, since our analytical method as so far developed is not yet suited to the calculation of the model motion with legs down.

In the case of a barge-type hull, it was found necessary to include surge motions, together with heaving and pitching. Since the barge has fore and aft symmetry, pitch, heave, and surge motions are in principle, indistinguishable from roll, heave, and sway. Consequently, pitch and surge hydrodynamics were calculated from Eqs. (2.10) for roll and sway. Hydrodynamic forces due to heave were evaluated with lengthwise strips.

The calculated heaving motions of the model are compared with the experimental values in Fig. 13A. For all practical purposes, the agreement is good enough. The prediction of pitching motion is also compared with the experimental results, in Figure 13B. The effects of theoretical and experimental dampings are also shown in the figure, where the formula used to define the experimental damping moment is

$$N_{\psi\psi} = \delta_1 \cdot \omega_{\psi} \cdot M_{\psi\psi}/\pi$$

where δ_1 = coefficient determined from the extinction curve of the model

ω_{ψ} = natural circular pitching frequency

$M_{\psi\psi}$ = pitching inertial moment coefficient (see second section of this report), determined theoretically

The prediction using the empirical damping moment is also seen to be in reasonably good agreement with the experiment (Fig. 13B).

For the surging motion, there are no experimental data presently available, but the calculation is shown in Fig. 13C. It is very interesting to note that the coupled effect appearing in the motion is significant. It is observable in the behavior of the curves of amplitude and phase near the natural pitching period.

Again using lengthwise strips, we investigated the surging and pitching motions in quartering seas ($\mu = 45^\circ$). These motions are illustrated in Figs. 14A and 14B. Both surging and pitching motions are generally smaller than the motions in head seas, but the curves show trends similar to those for head seas.

HEAVING, SWAYING, YAWING, AND ROLLING MOTIONS

Although we have not obtained the experimental data for the rolling motions of this jackup rig model, the calculation of the motions was carried out for beam seas ($\mu = 90^\circ$) and quartering seas ($\mu = 45^\circ$). The vertical coupled Eqs. (3.1) with transverse strips are utilized for determining the heaving motion in beam seas ($\mu = 90^\circ$). The lateral coupled Eqs. (3.3) are solved to determine swaying, yawing, and rolling motions for these cases. The heaving motion of the model in beam seas is illustrated in Fig. 15A. The motion amplitude reaches the maximum in a shorter wave than in head-sea motion. The swaying motion is shown in Fig. 15B. The tendency of the motion is similar to that of the surging motion of the model in head seas. The natural rolling period was not measured in the experiment, and the natural period cannot be pin-pointed, but the fluctuation should occur near the natural period. This is expected from the foregoing investigation of pitch and surge in head seas. The rolling motion is shown in Fig. 15C. It is evidently larger than the pitching motion. It should be noted, however, that the motion was calculated by employing only the wave-making damping. Including viscous damping as determined from a roll-extinction test should reduce the predicted roll motion, but further calculations await additional experimental measurements.

The lateral motions in oblique seas ($\mu = 45^\circ$) are illustrated in Figs. 16A, 16B and 16C. The swaying and rolling motions are smaller than those in beam seas, as might be expected. The yawing motion amplitude is certainly much smaller than the other two motions, and increases as the wavelength-to-ship length ratio λ/L increases.

CONCLUSIONS AND RECOMMENDATIONS

An analytical procedure has been derived and evaluated for predicting motions in six degrees of freedom for floating vehicles with no forward speed. This procedure was applied to conventional ship-type hulls and to barge-type hulls representing jackup drill rigs. Predicted results were found to be in good agreement with those corresponding measured results that are presently available.

The analytical procedure is based on the use of two-dimensional strip theory to represent the hydrodynamic forces and moments acting on the hull. These loads are assumed directly proportional to sinusoidal wave amplitude at each frequency, and the flow is assumed inviscid except in the case of roll for conventional ship forms and in the case of roll and pitch for barges. In the latter case, viscous linear damping moments are required, but in the former case, viscous linear and quadratic damping moments were found necessary. The viscous damping moments were characterized empirically from the results of roll or pitch extinction measurements when available.

Some further experimental work is required to increase the degree of reliability of the analytical procedures derived here. At present, however, the procedure is considered sufficiently reliable for conceptual design-stage studies of motions and loads for ocean platforms.

In a continuing effort to derive useful reliable design-stage techniques for ocean-platform analysis, future studies will be carried out to include a variety of practical effects in this prediction capability. Some of these are:

- (1) Hydrodynamic forces on vertical cylindrical legs
- (2) Dynamic constraints due to mooring lines
- (3) Calculation of wave-induced and motion-induced bending moments

In connection with the first of these recommendations, some experimental work has been carried out. Results are shown in Fig. 17, with wave period extrapolated to full scale.

The procedures will be further extended to include other types of ocean platforms such as semi-submersibles and buoys. Since proposed buoy shapes vary widely, the results for mathematical shapes from References 10 and 11 may not be of practical use.

Another effect that has practical importance appertains to the drifting motion and loads which can be calculated by means of a straightforward extension of the procedure already developed.

ACKNOWLEDGEMENTS

The authors are indebted to Dr. J. P. Breslin, Mr. E. Numata, and Dr. C. J. Henry, for their expressions of interest and advice during the period of research.

REFERENCES

1. FRANK, W., "On the Oscillation of Cylinders in or Below the Free-Surface of Deep Fluids," NSRDC Report 2375, Oct. 1967.
2. GRIM, O., "Eine Methode für eine genauere Berechnung der Tauch- and Stampfbewegungen in glattem Wasser und in Wellen," HSVA-Bericht Nr. 1217, June 1960.
3. TAMURA, K., "The Calculation of Hydrodynamical Forces and Moments Acting on the Two-Dimensional Body - According to Grim's Theory," Jour. SZK, No. 26, Sept. 1963.
4. GRIM, O. and SCHENZLE, P., "Berechnung der Torsionsbelastung eines Schiffes im Seegang," Forschungszentrum des Deutschen Schiffbaus, Bericht Nr. 5, 1968.
5. WEHAUSEN, J.V. and LAITONE, E.V., "Surface Waves," Handbuch der Physik, Band IX, Springer Verlag 1960.
6. KIM, C.H. and CHOU, F., "Wave-Exciting Forces and Moments on an Ocean Platform Fixed in Oblique Seas," Offshore Technology Conference, No. 1180, April 1970, Houston, Texas.
7. TASAI, F., "Ship Motions in Beam Seas," Report of Research Institute for Applied Mechanics, Kyushu University, Vol. XIII, No. 45, 1965.
8. VOSSERS, G., "Behavior of Ships in Waves," Resistance, Propulsion and Steering of Ships, Technical Publishing Co., H. Stam, N.V. Haarlem (the Netherlands), 1962.
9. TASAI, F., "On the Swaying, Yawing and Rolling Motions of Ships in Oblique Waves," International Shipbuilding Progress, Vol. 14, No. 153, May 1967.
10. HAVELOCK, T.V., "Waves Due to a Floating Sphere Making Periodic Heaving Oscillations," Proceedings, Royal Soc London, Vol. 231, Series A, 1955.
11. KIM, W.D., "On a Free-Floating Ship in Waves," J. Ship Research, Vol. 10, No. 3, Sept. 1966.

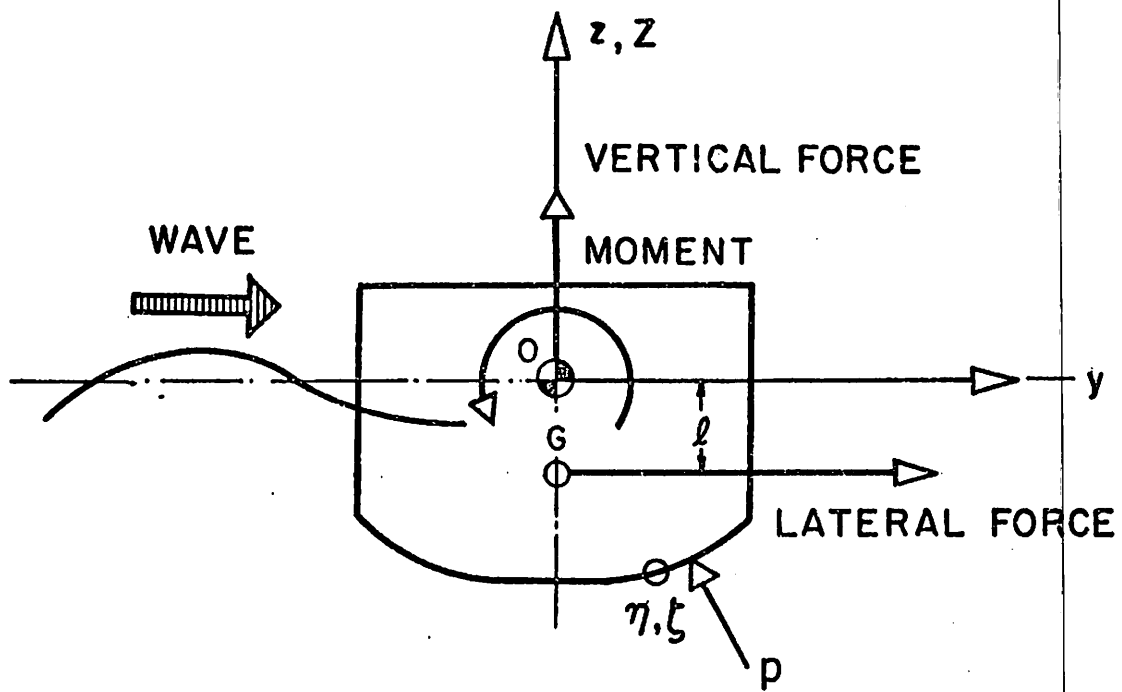


FIG. 1A. STRIP SECTION

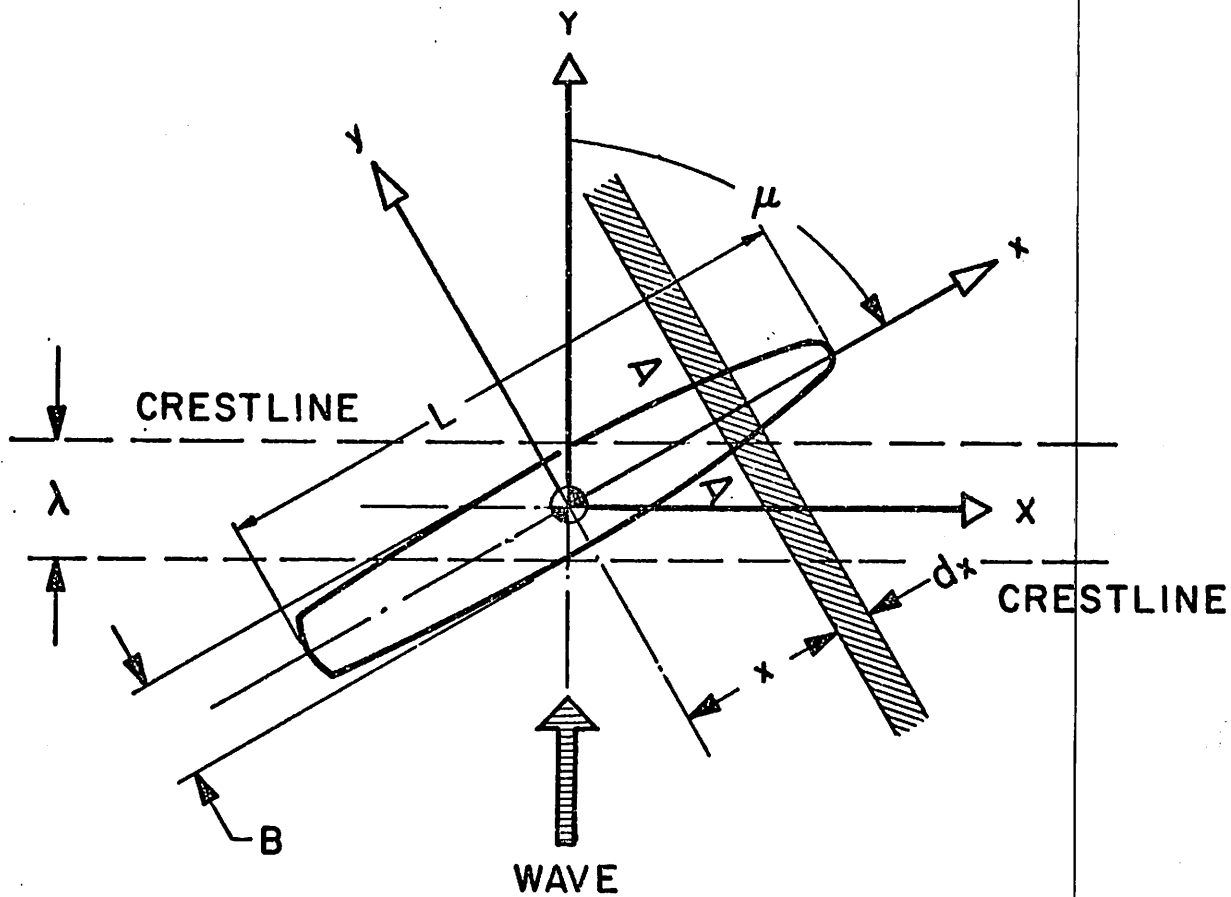


FIG. 1B. COORDINATE SYSTEMS

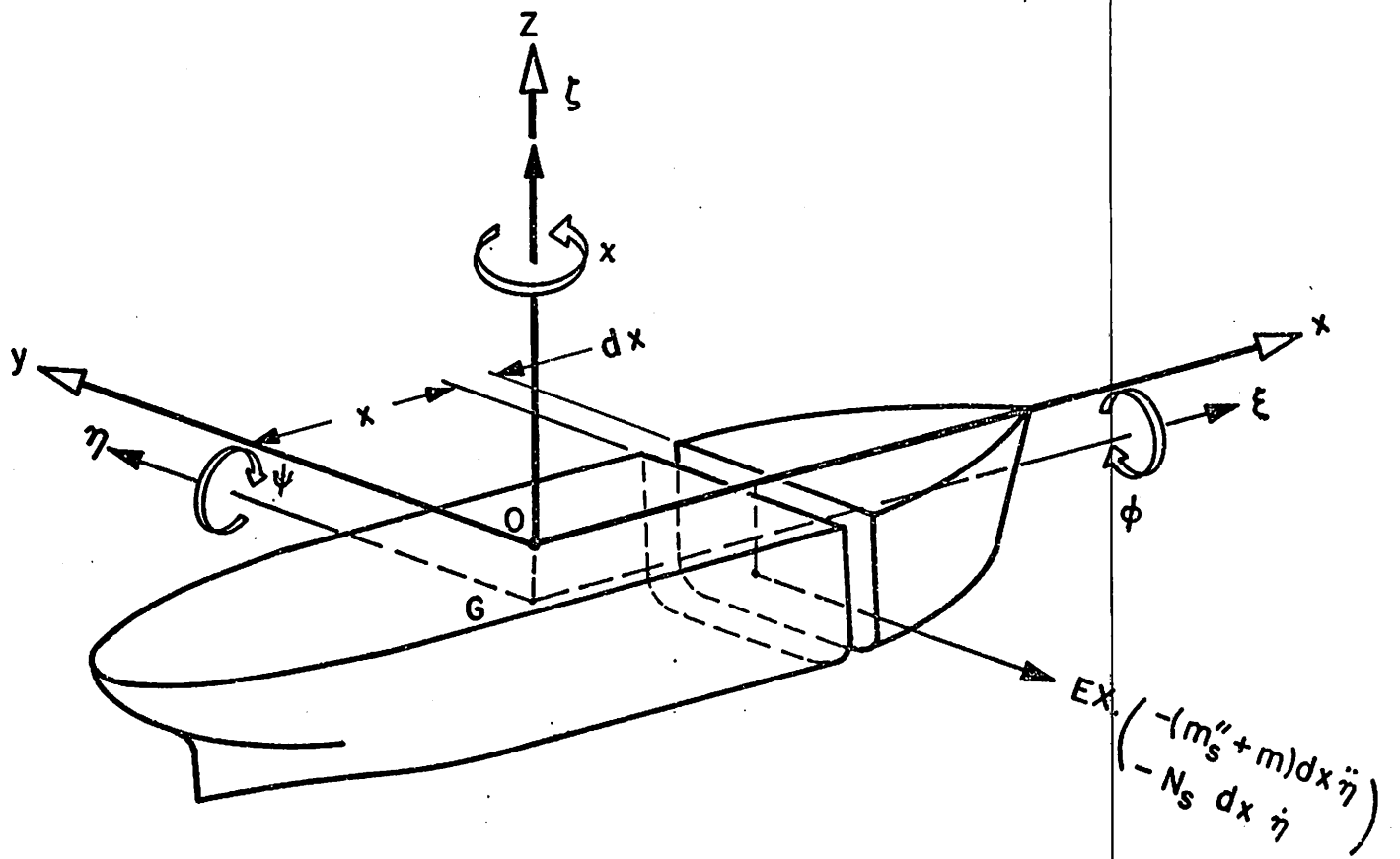


FIG. IC. DEFINITION OF FORCES AND MOMENTS

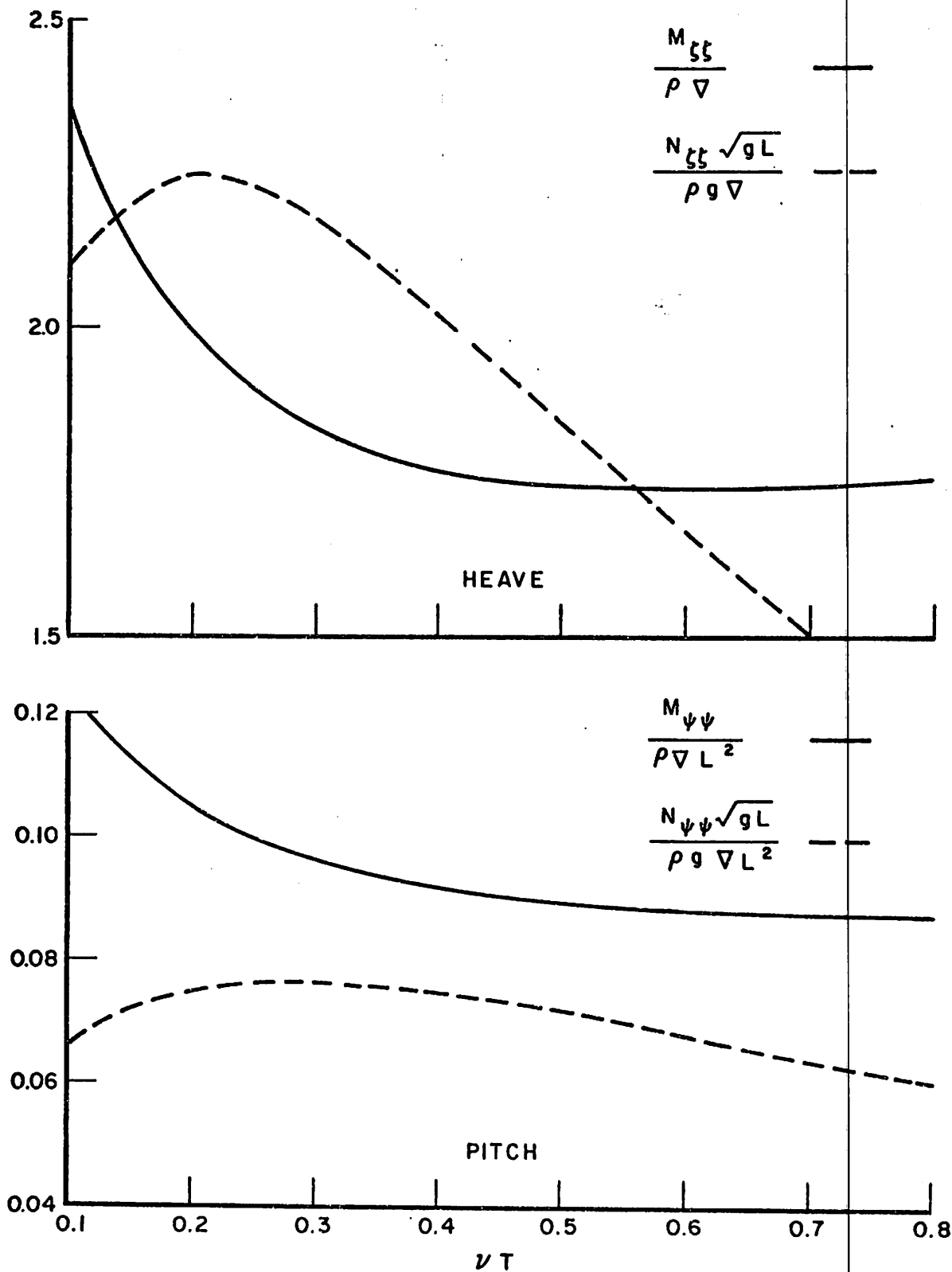


FIG. 2. HEAVING AND PITCHING INERTIAL AND DAMPING COEFFICIENTS OF SHIP MODEL

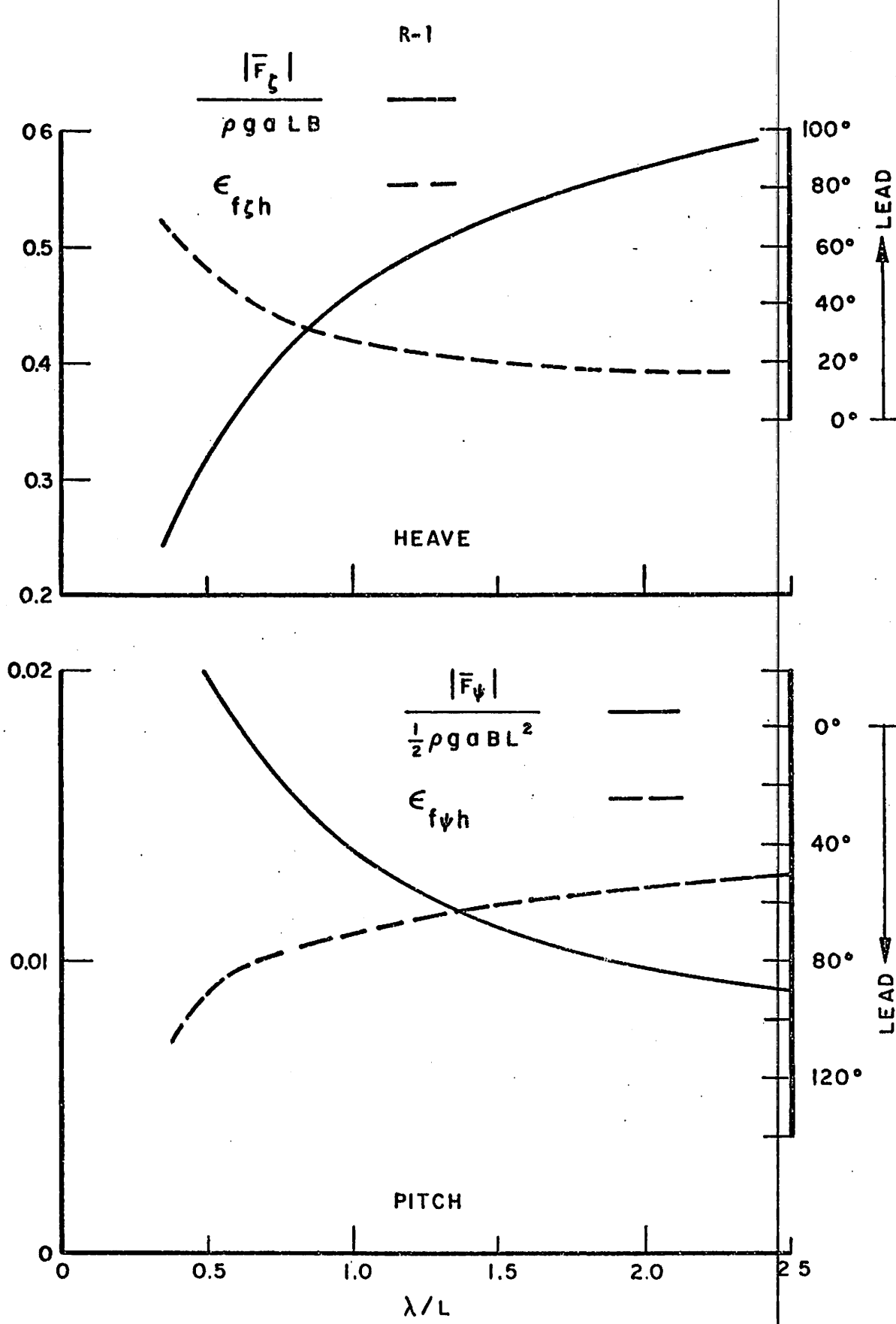


FIG. 3. HEAVE-AND PITCH-EXCITING FORCE AND MOMENT ON SHIP MODEL IN BEAM SEAS ($\mu = 90^\circ$)

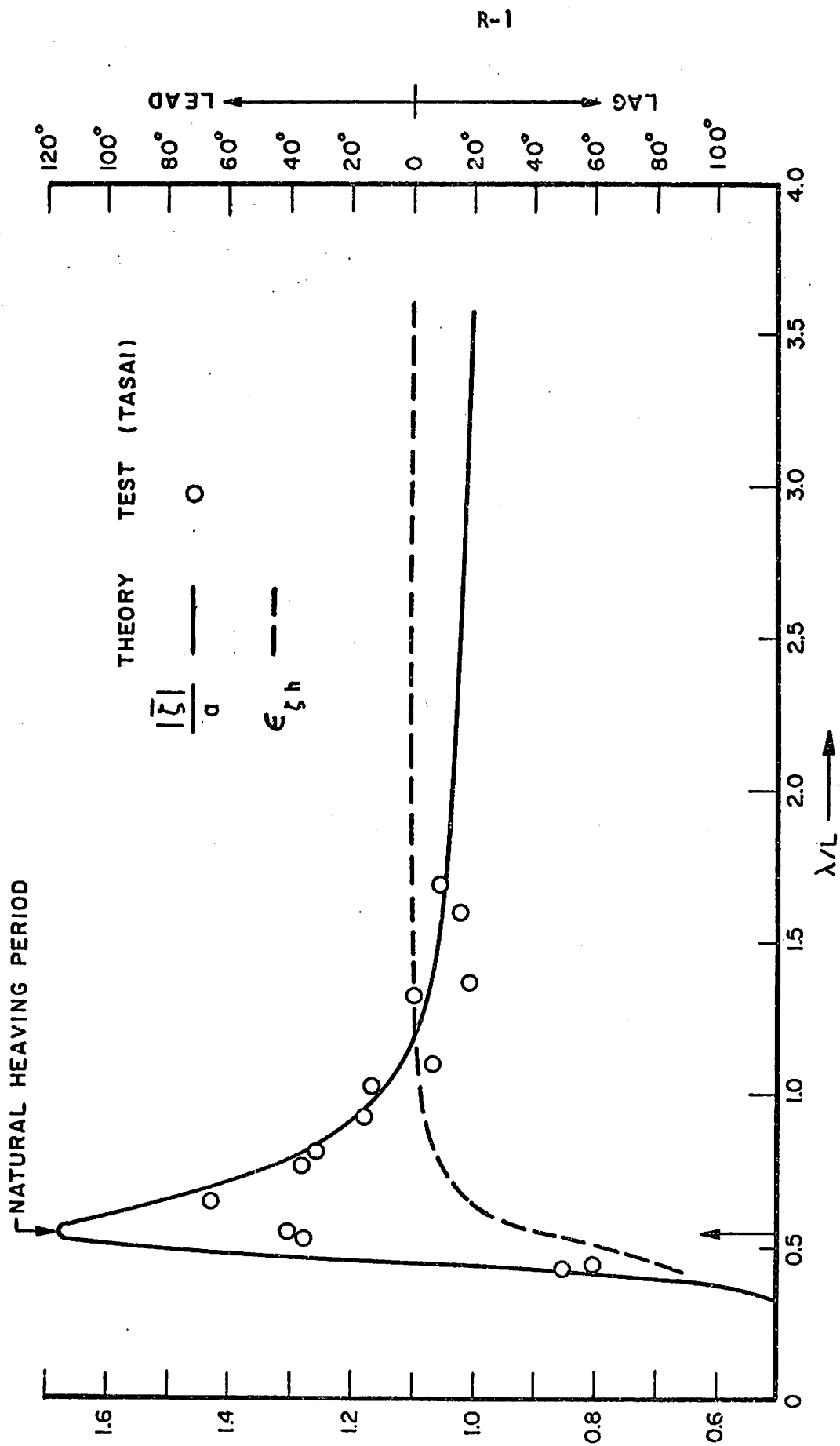


FIG. 4A. HEAVING MOTION OF SHIP MODEL IN BEAM SEAS ($\mu = 90^\circ$)

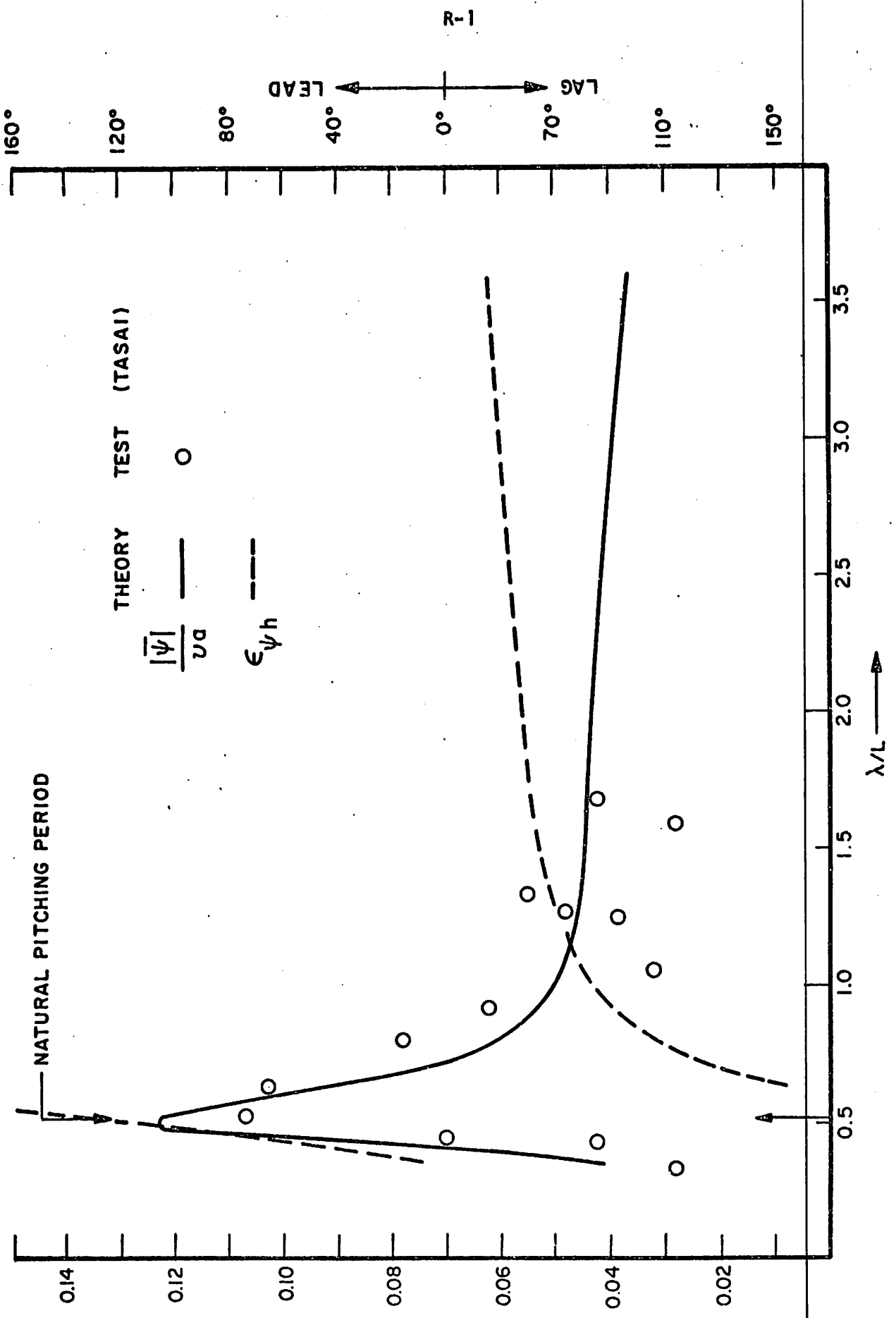


FIG.4B. PITCHING MOTION OF SHIP MODEL IN BEAM SEAS ($\mu = 90^\circ$)

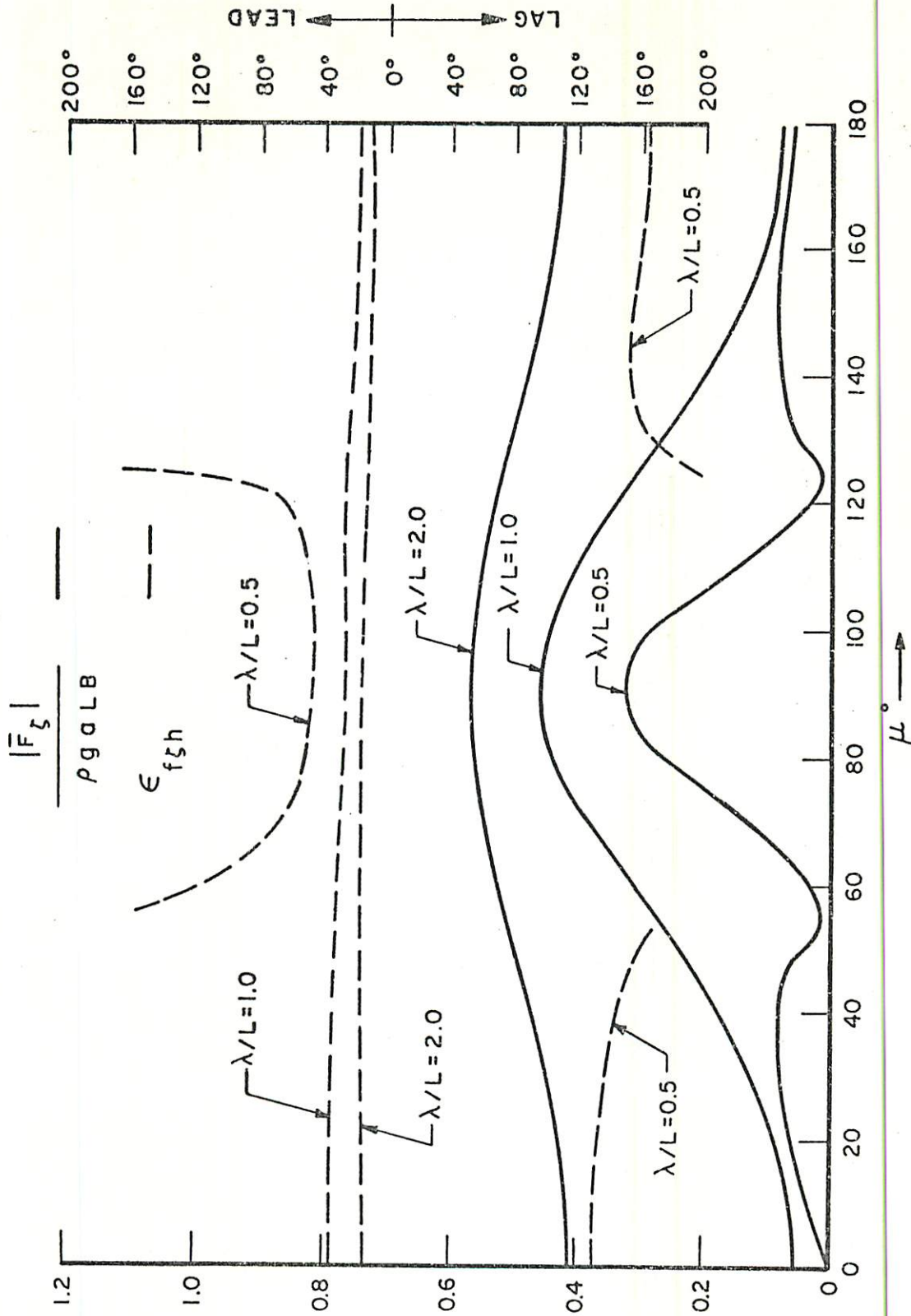


FIG. 5A. HEAVE-EXCITING FORCE ON SHIP MODEL IN OBLIQUE SEAS

$$\frac{|\bar{F}_\psi|}{\frac{1}{2} \rho g a B L^2} \quad \text{---}$$

$$\epsilon_{f\psi h} \quad \text{- - -}$$

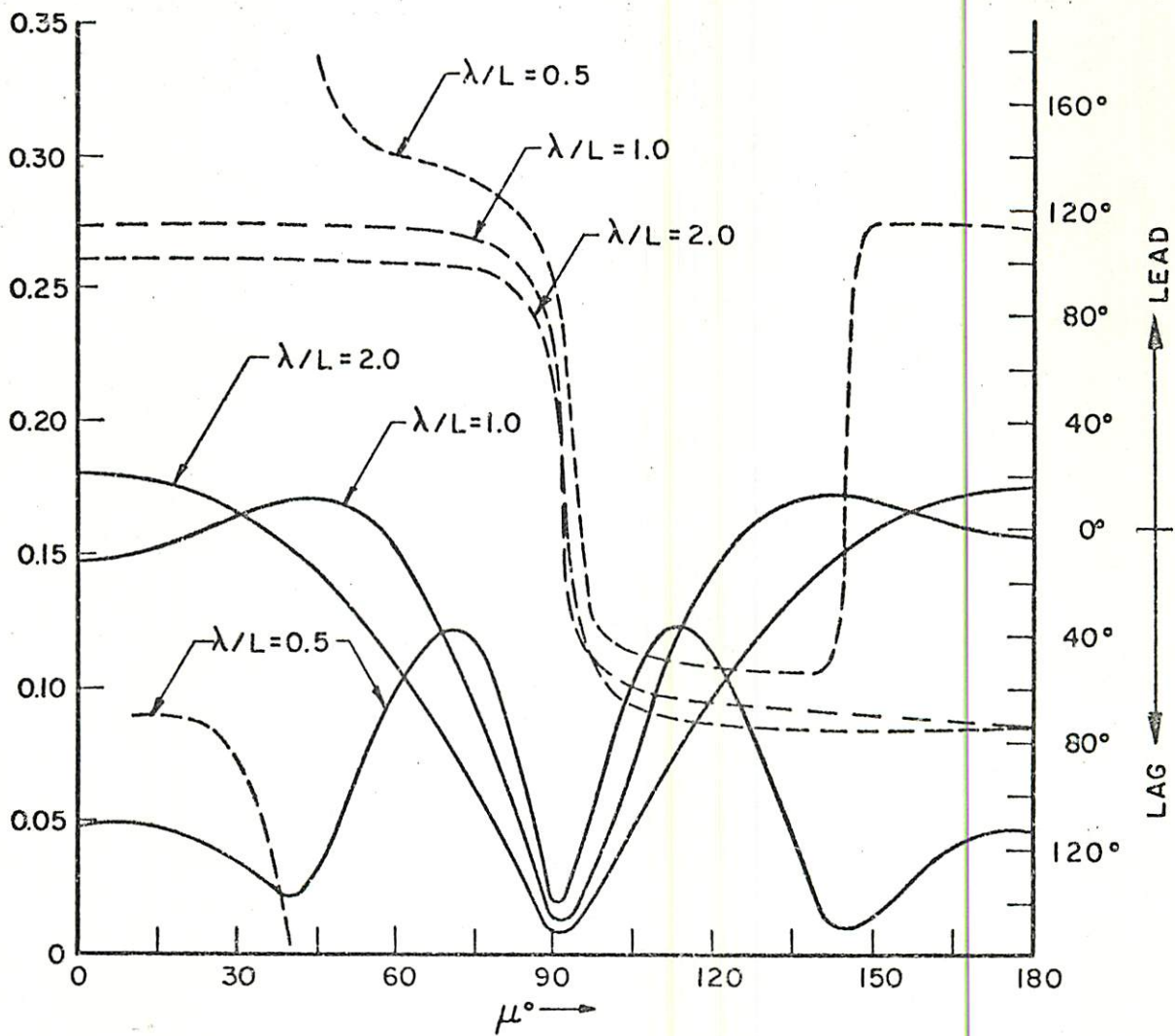


FIG. 5B. PITCH-EXCITING MOMENT ON SHIP MODEL IN OBLIQUE SEAS

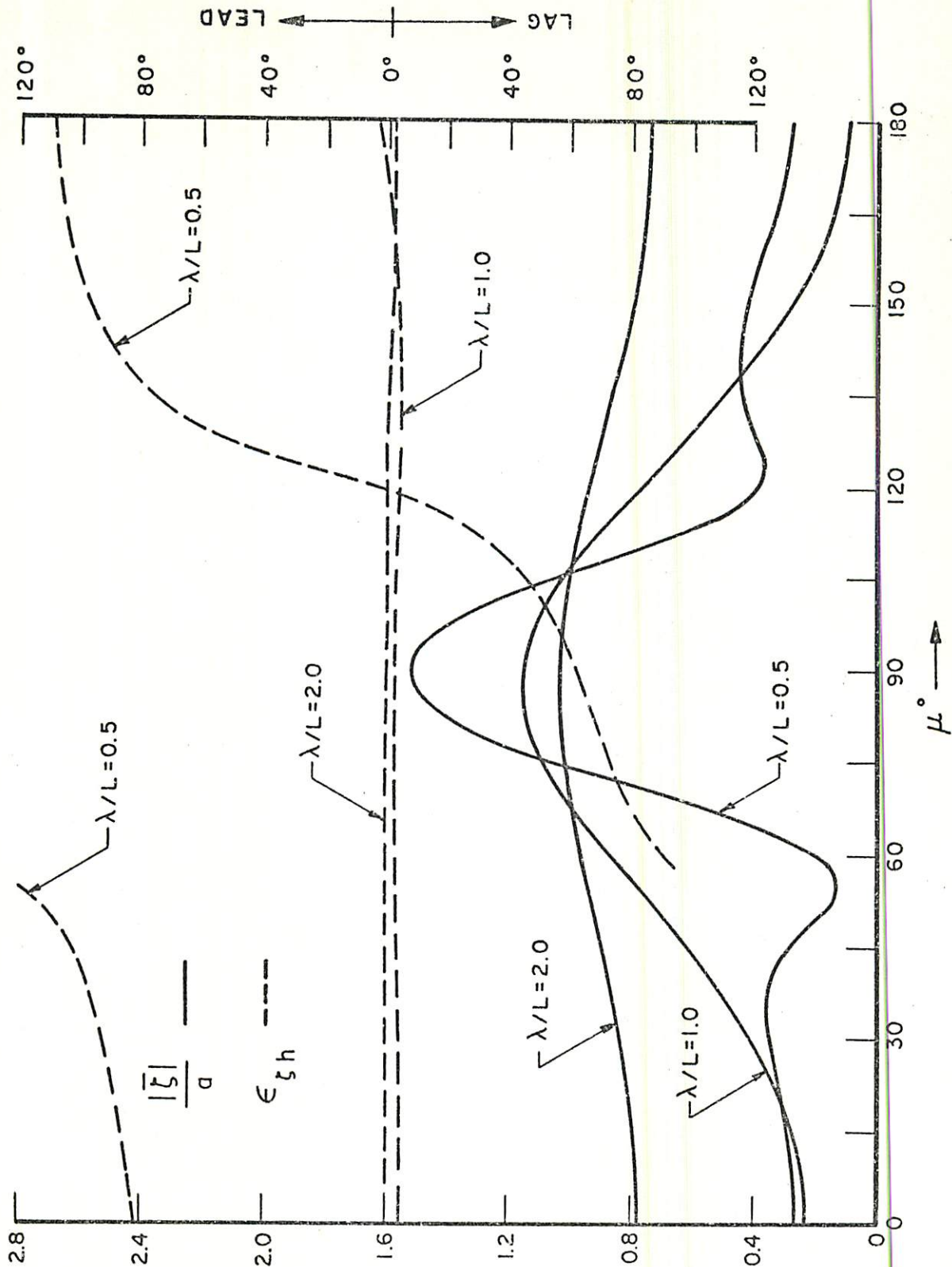


FIG. 6A. HEAVING MOTION OF SHIP MODEL IN OBLIQUE SEAS

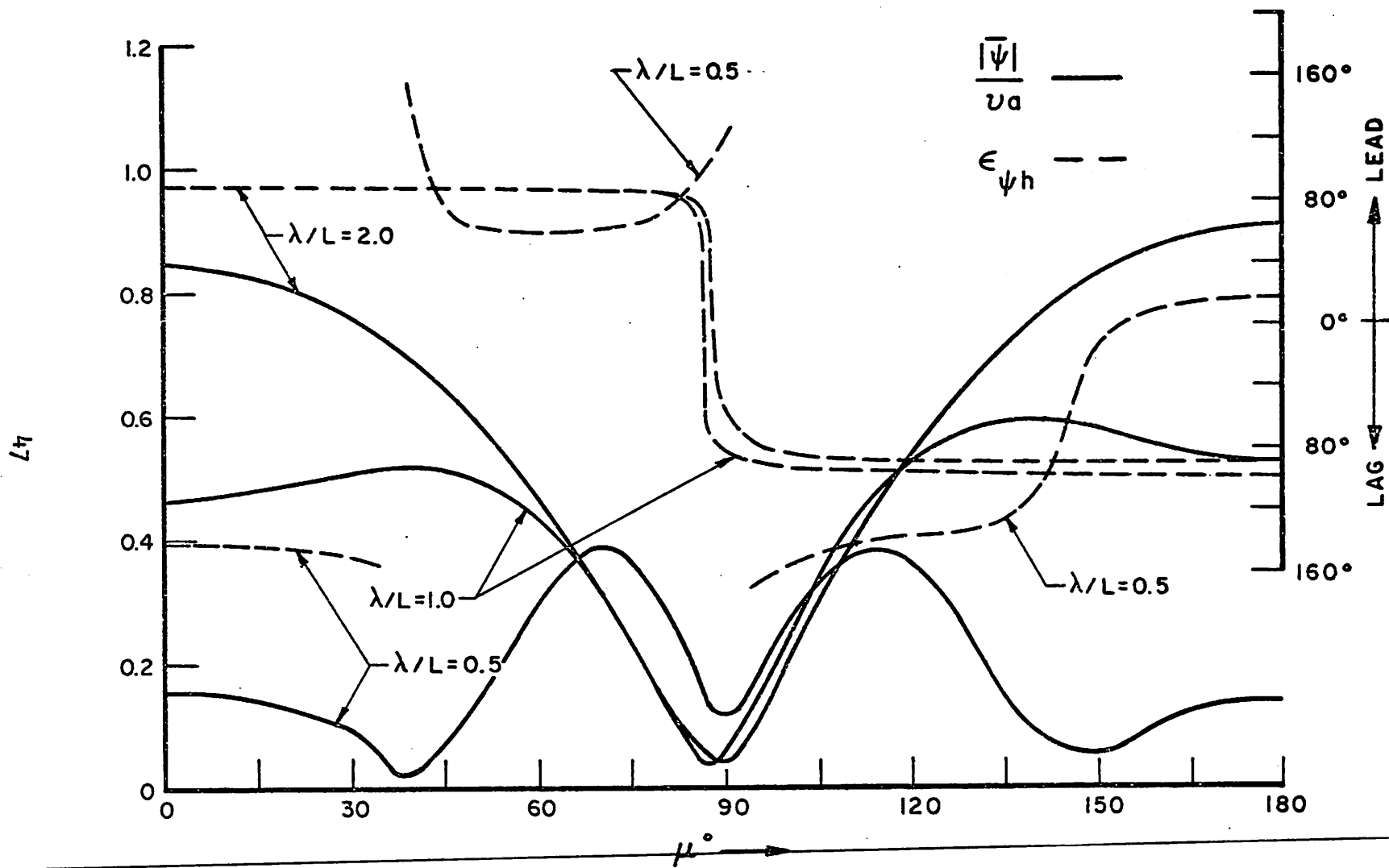


FIG. 6B. PITCHING MOTION OF SHIP MODEL IN OBLIQUE SEAS

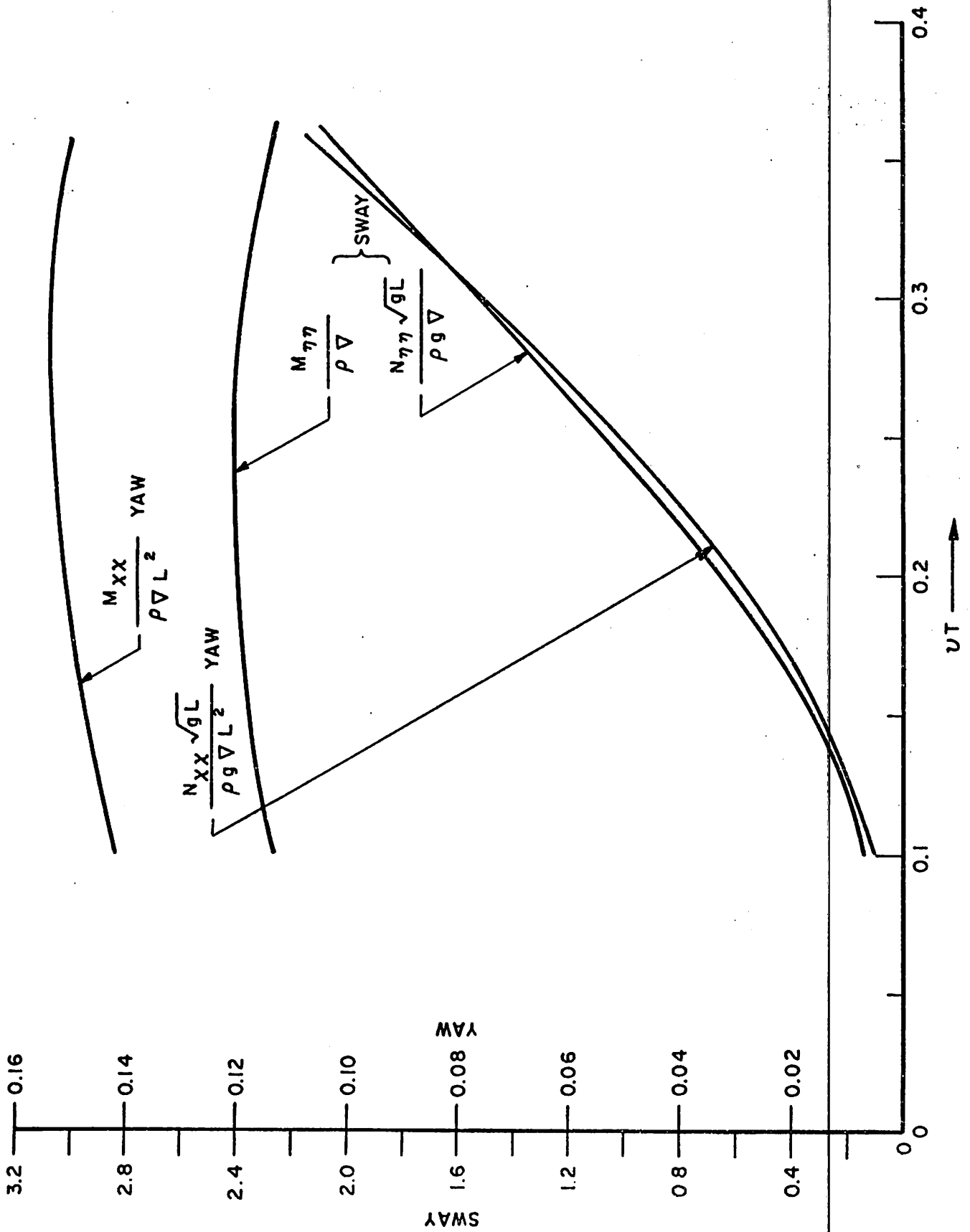


FIG. 7A. SWAYING AND YAWING INERTIAL AND DAMPING COEFFICIENTS OF SHIP MODEL

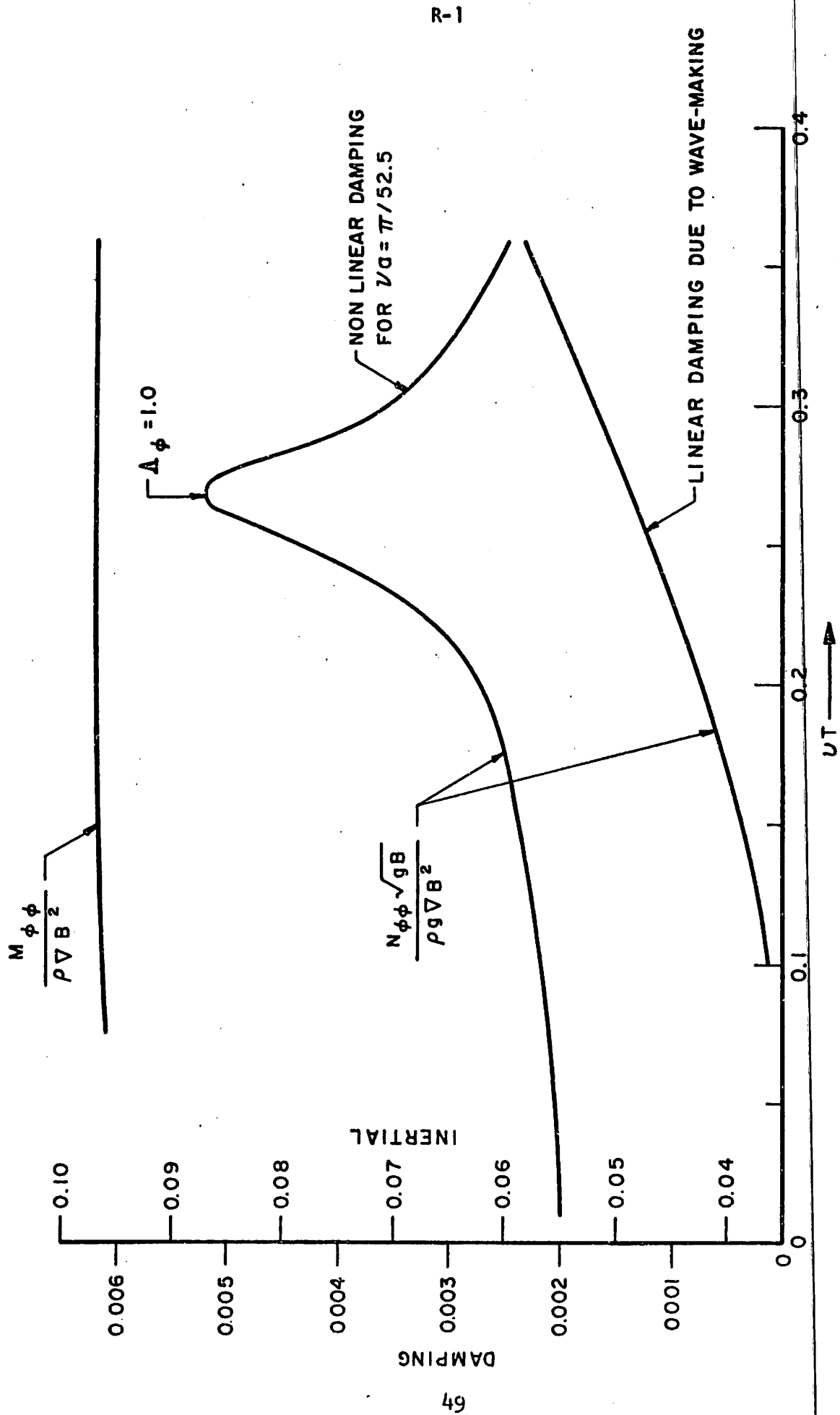


FIG. 7B. ROLLING INERTIAL AND LINEAR AND NON-LINEAR DAMPING COEFFICIENTS OF SHIP MODEL

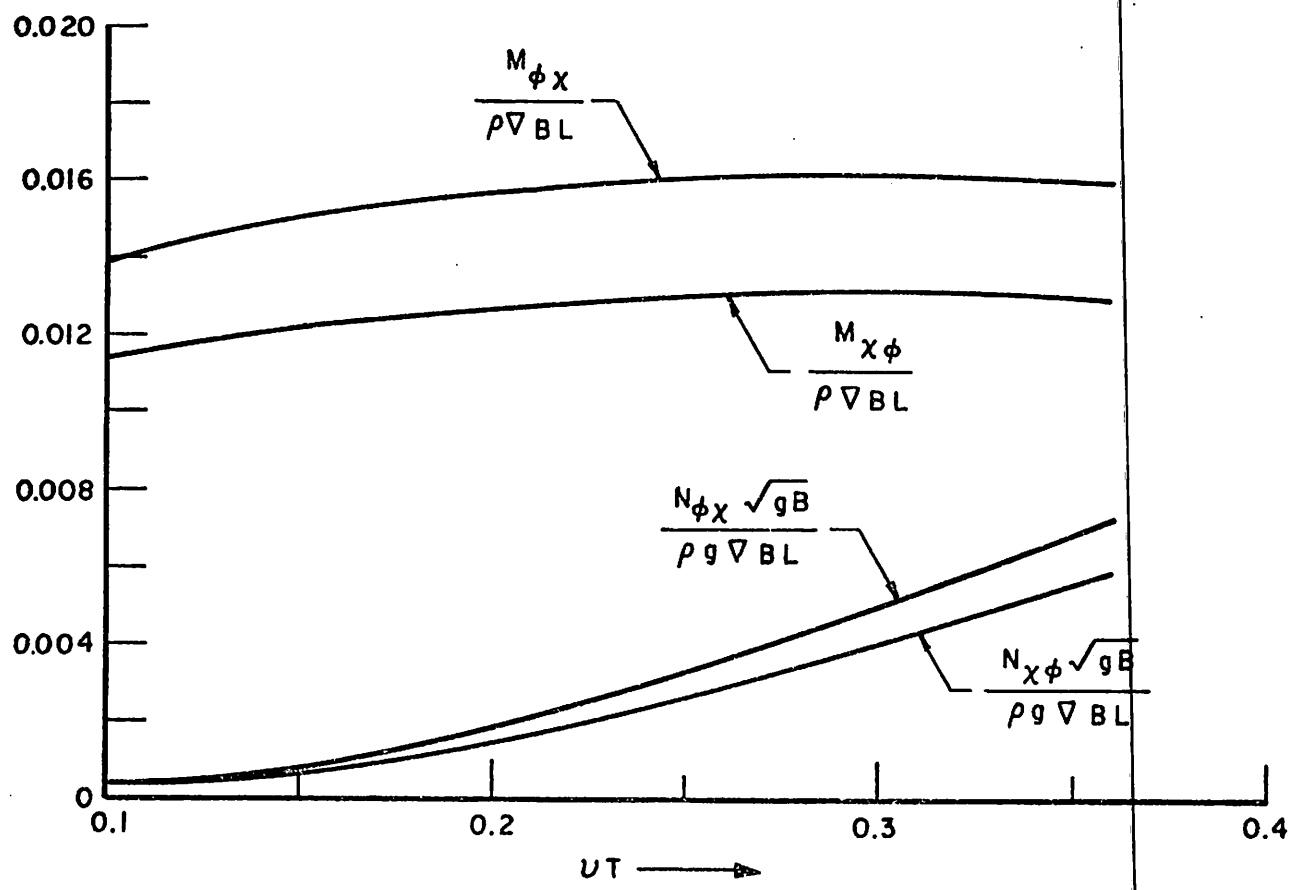
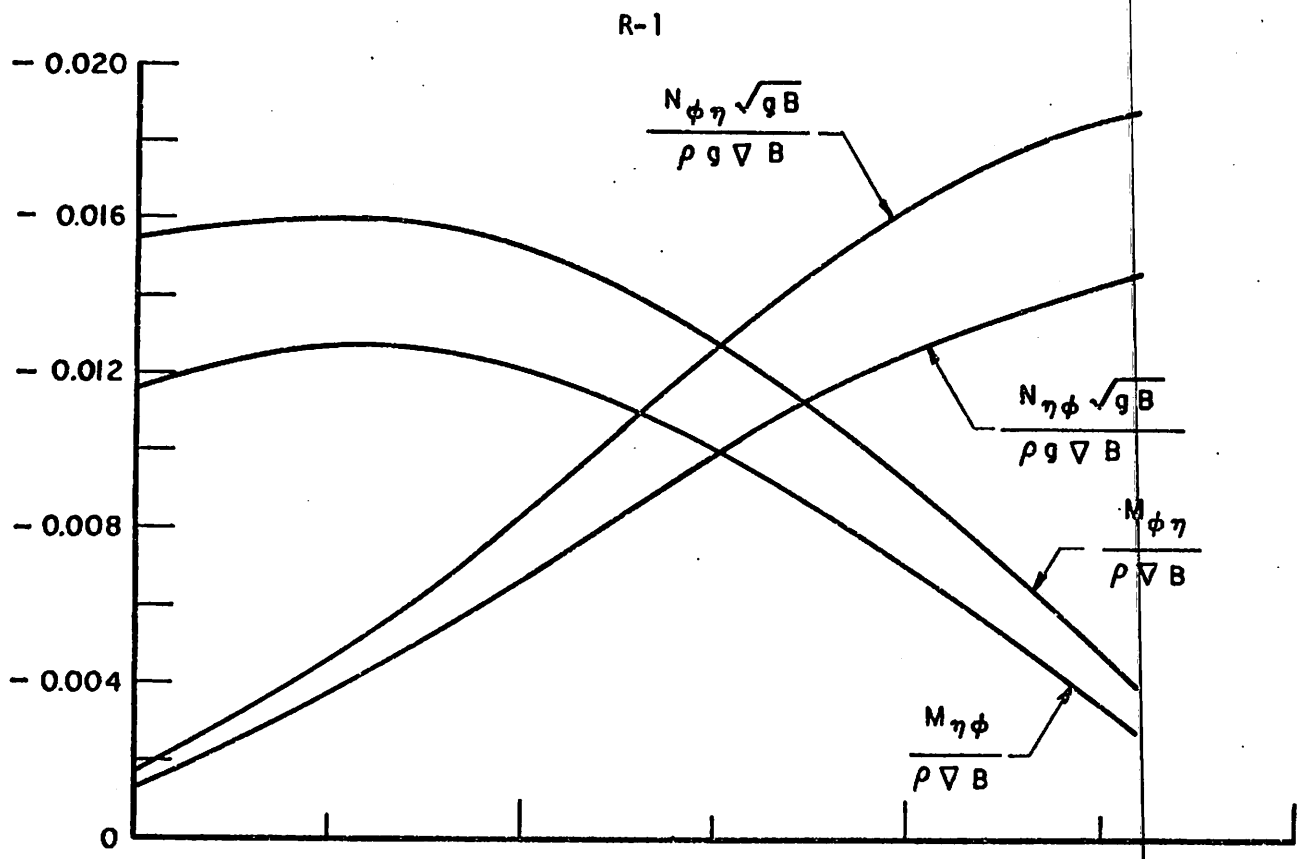


FIG. 7C. COUPLING INERTIAL AND DAMPING COEFFICIENTS OF SHIP MODEL

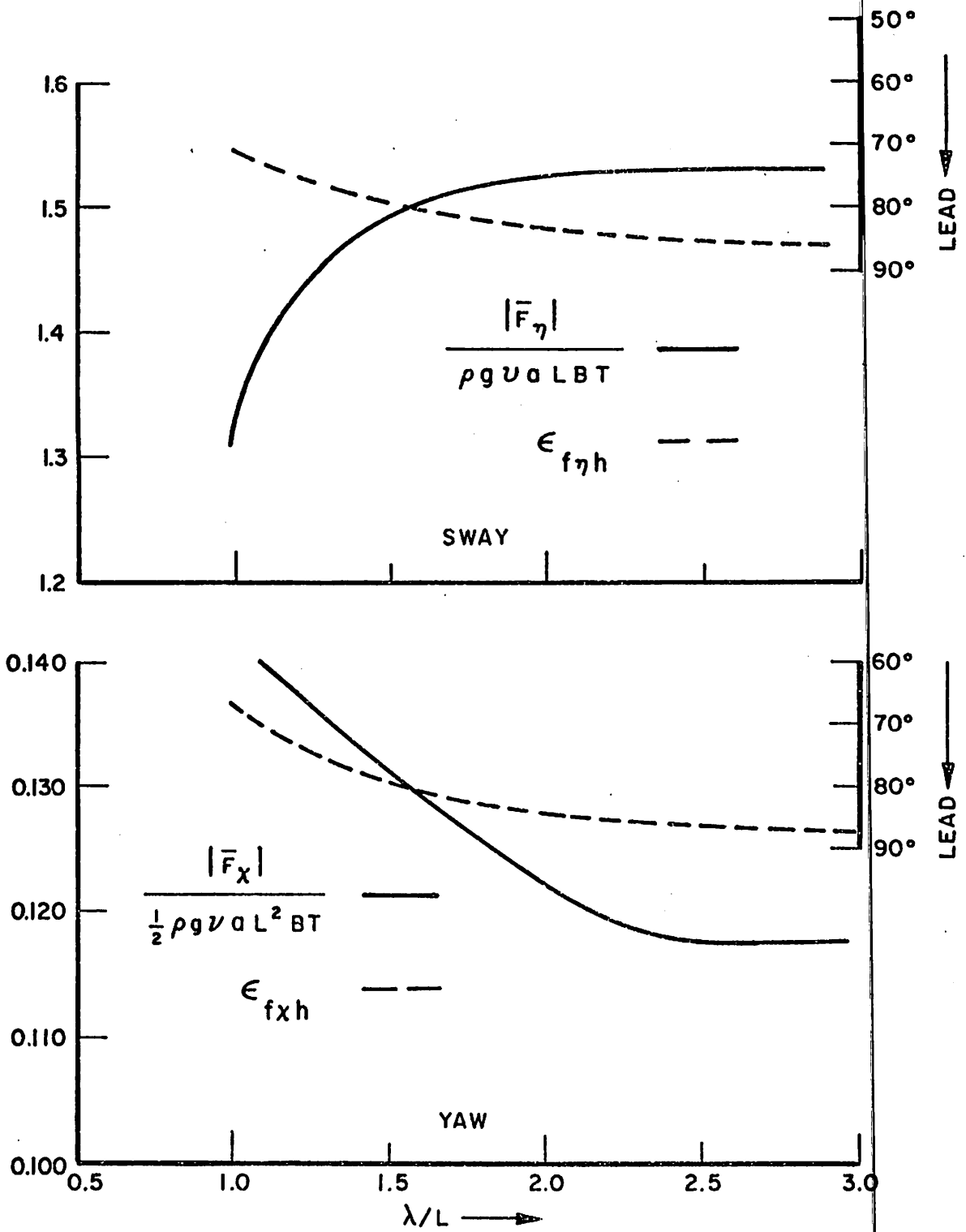


FIG. 8A. SWAY-AND YAW-EXCITING FORCE AND MOMENT ON SHIP MODEL IN BEAM SEAS ($\mu = 90^\circ$)

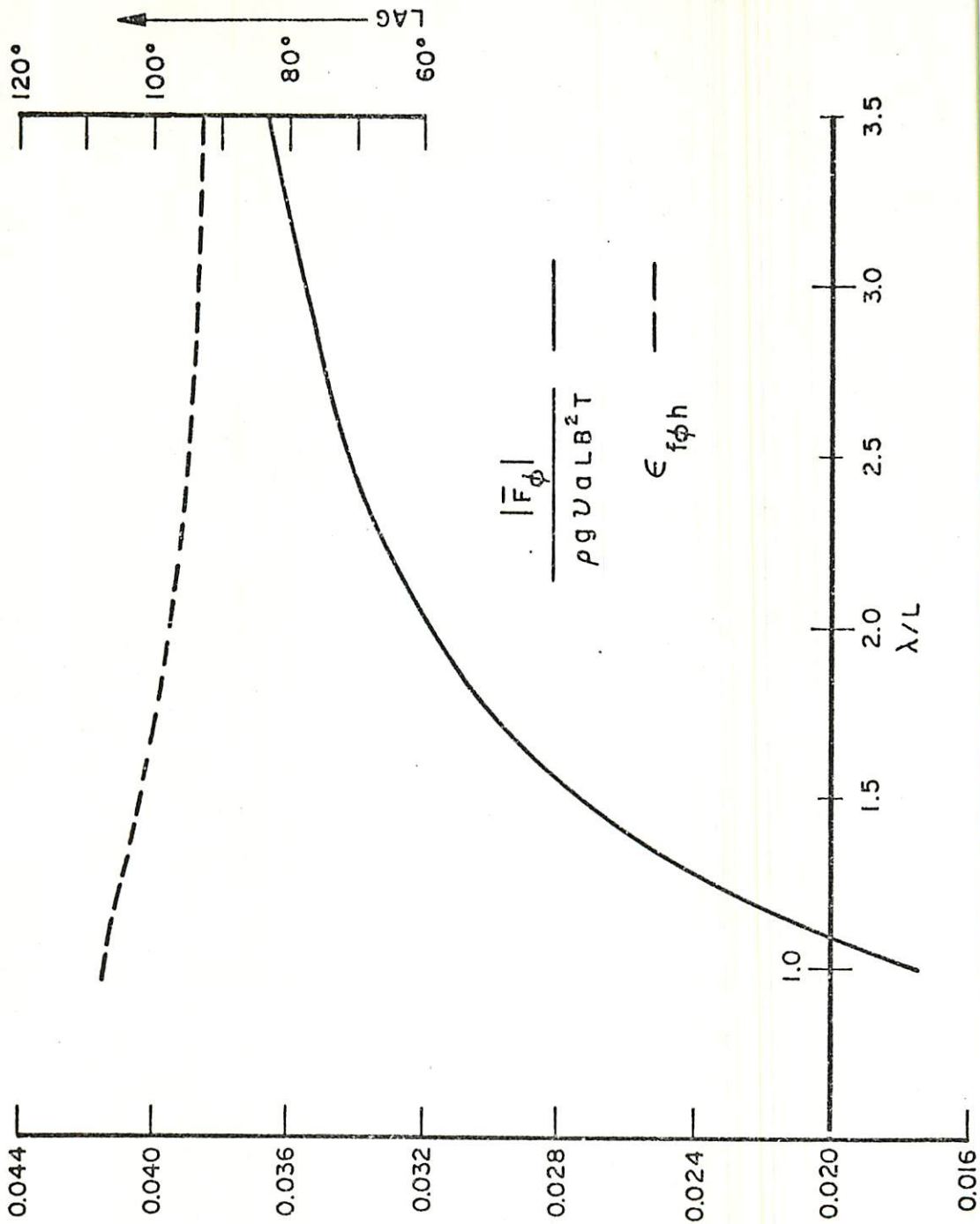


FIG. 8B. ROLL-EXCITING MOMENT ON SHIP MODEL IN BEAM SEAS ($\mu = 90^\circ$)

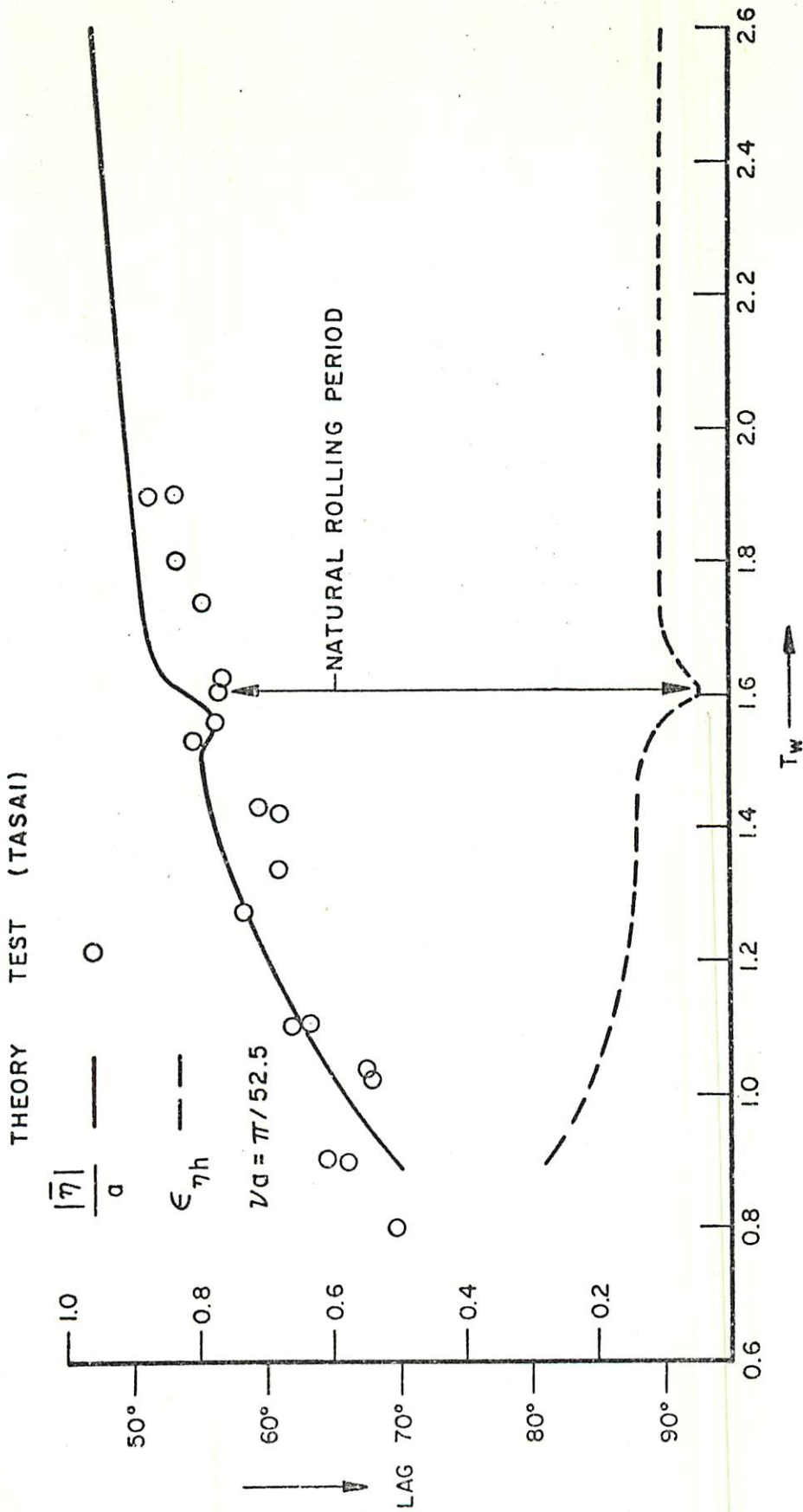


FIG. 9A. SWAYING MOTION OF SHIP MODEL IN BEAM SEAS ($\mu = 90^\circ$)

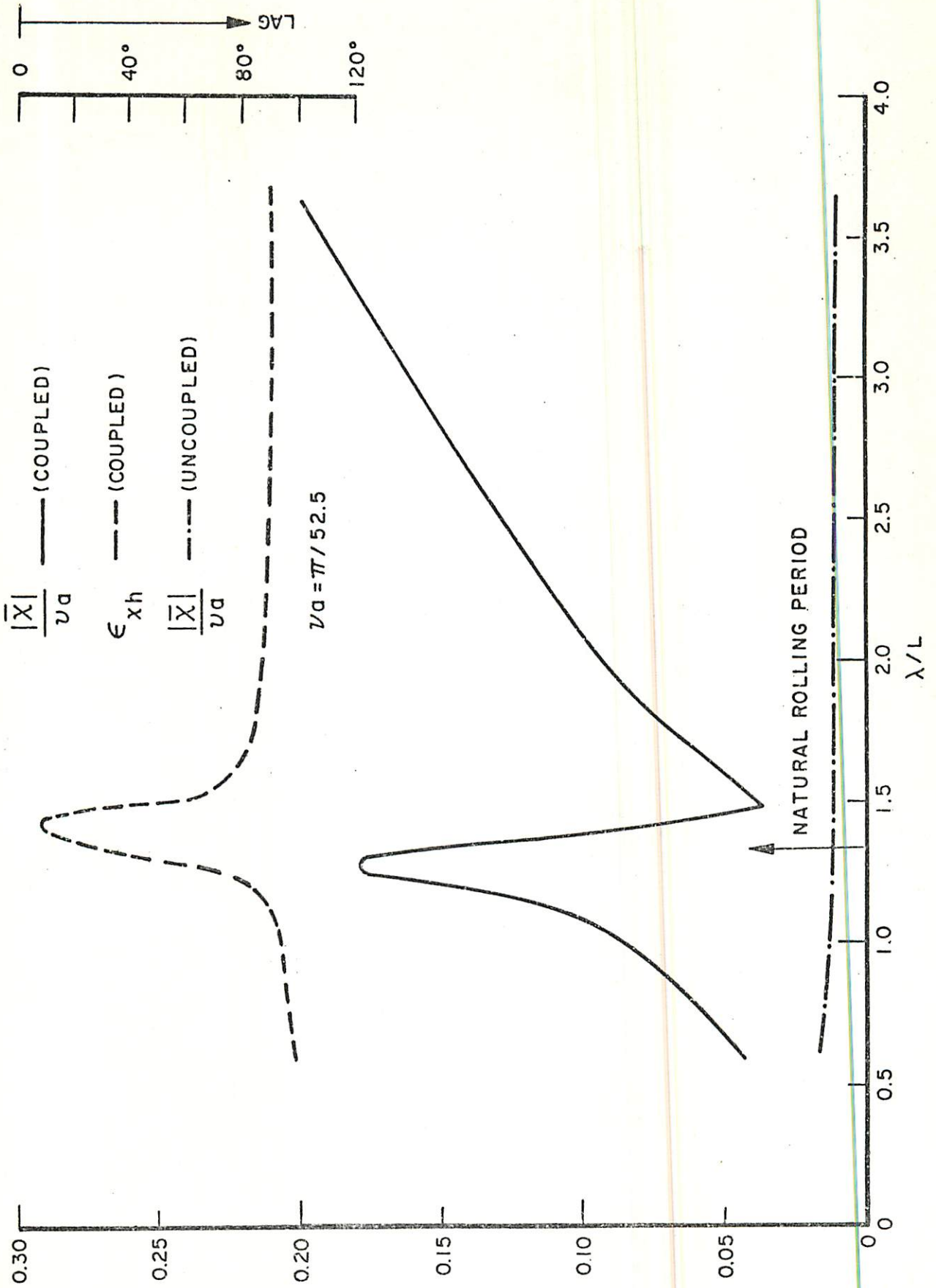


FIG. 9B. YAWING MOTION OF SHIP MODEL IN BEAM SEAS ($\mu = 90^\circ$)

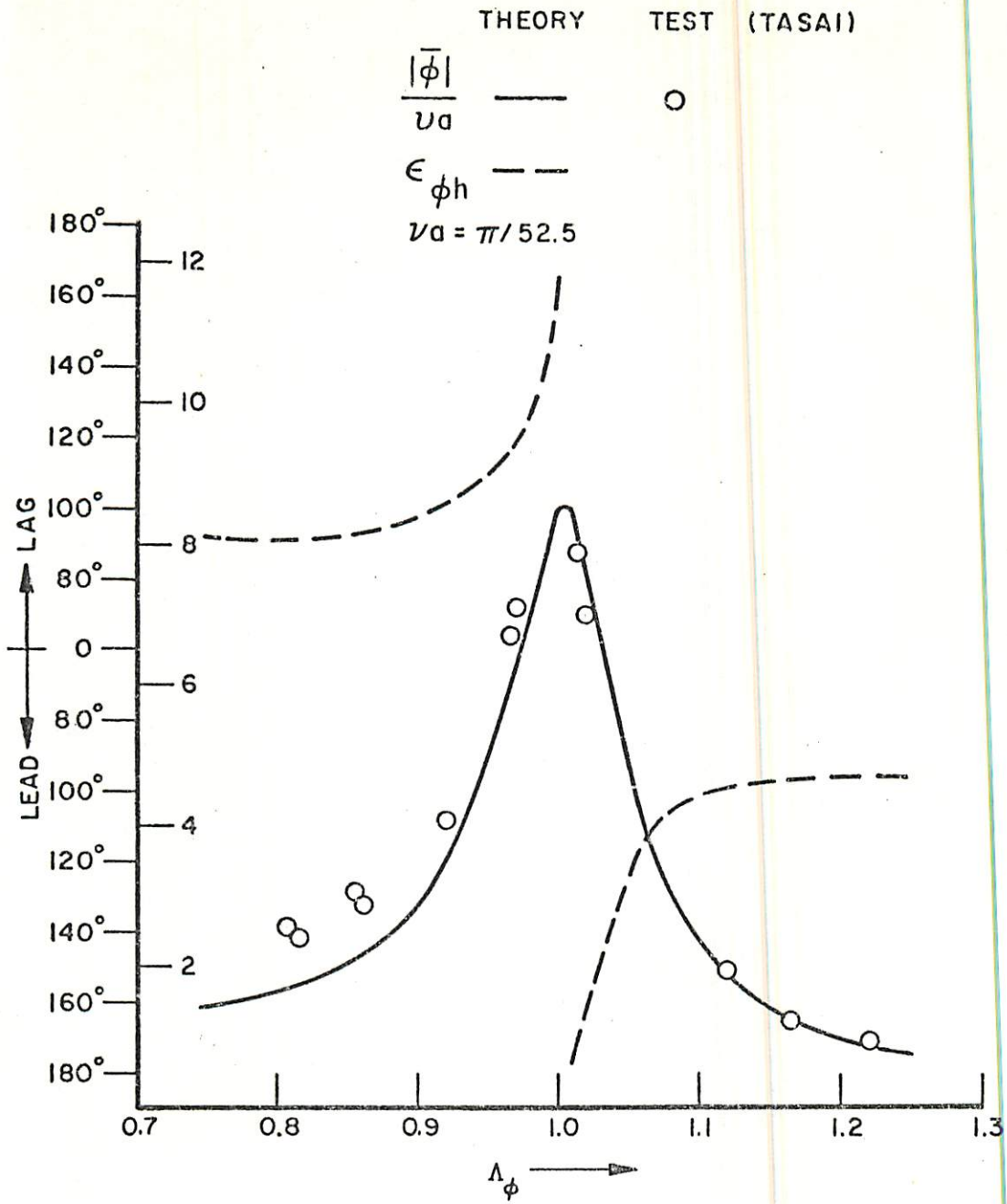


FIG. 9C. ROLLING MOTION OF SHIP MODEL IN BEAM SEAS ($\mu = 90^\circ$)

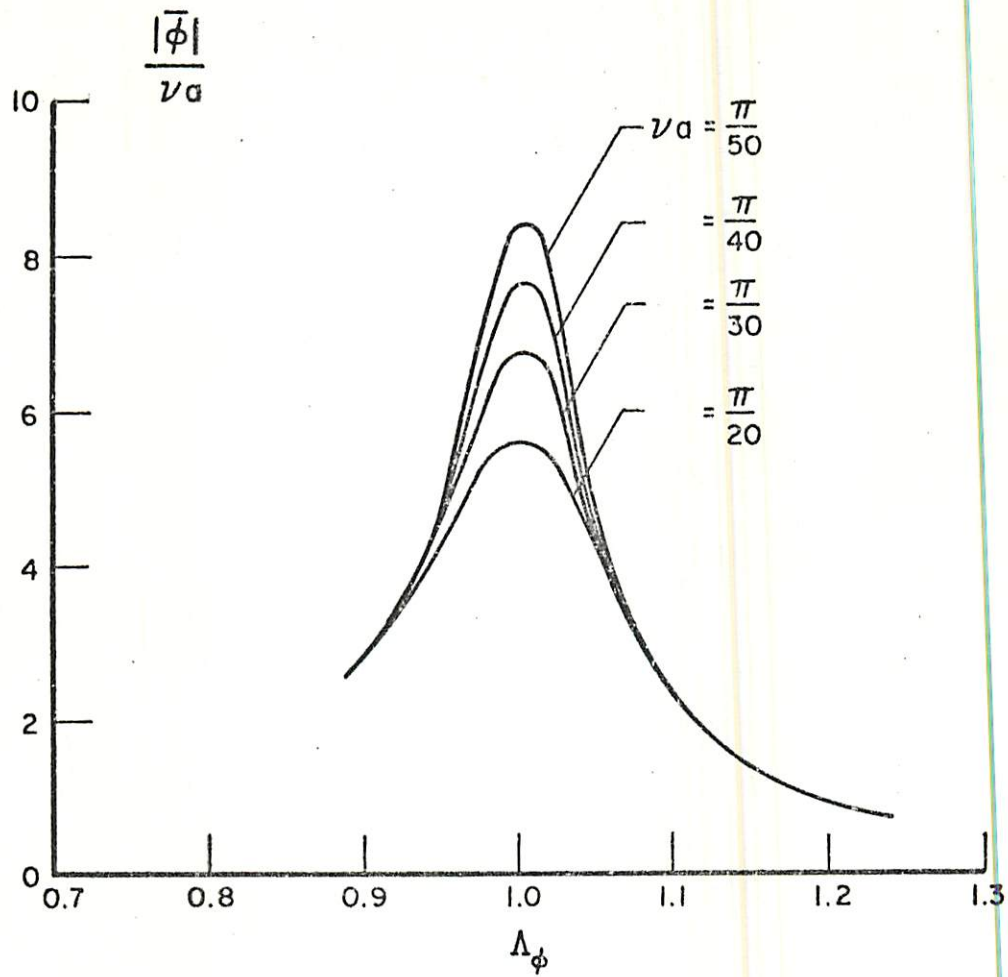


FIG. 9D. EFFECT OF THE WAVE SLOPE ON THE ROLL MOTIONS IN BEAM SEAS ($\mu = 90^\circ$)

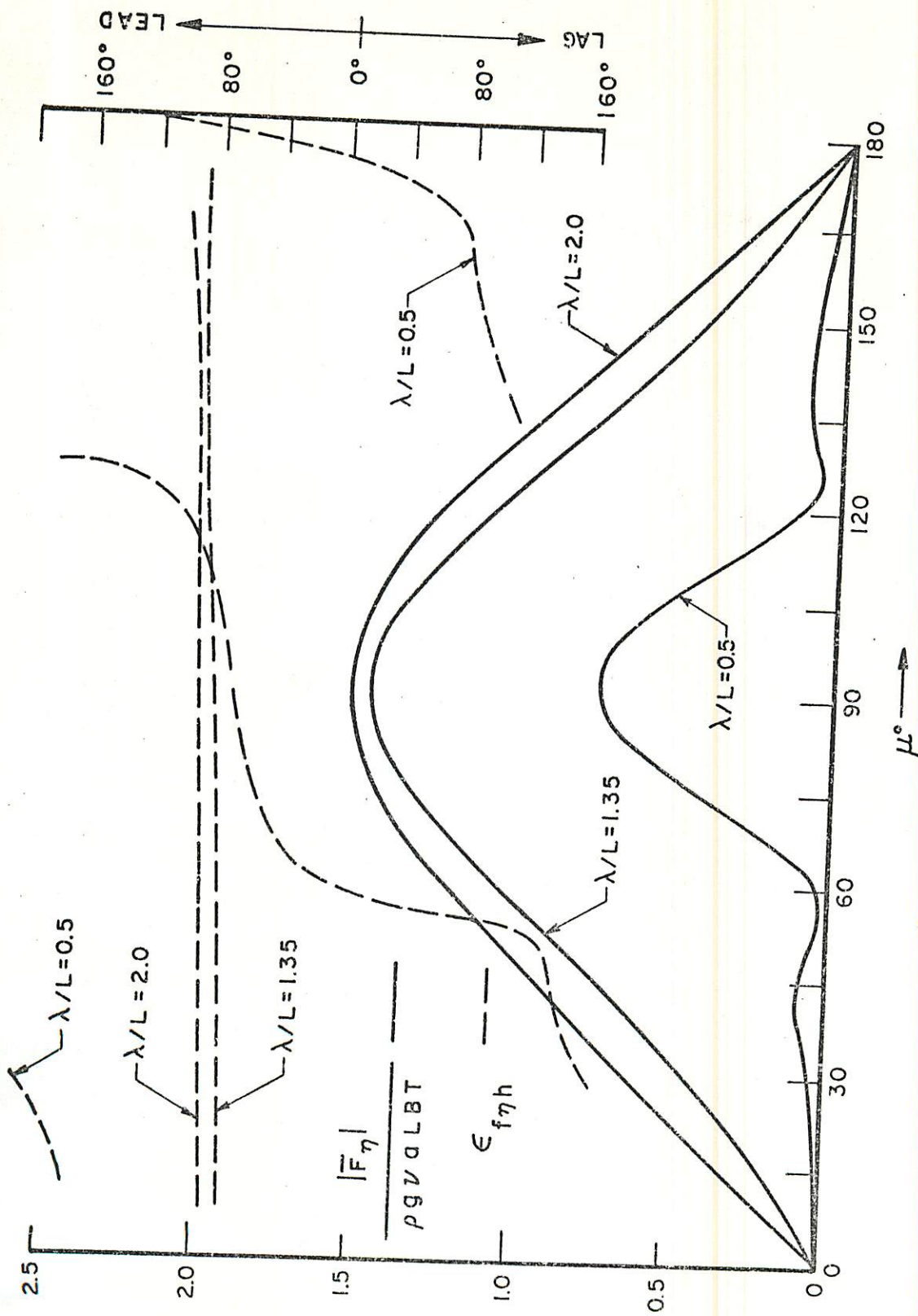


FIG.10A. SWAY-EXCITING FORCE ON SHIP MODEL IN OBLIQUE SEAS

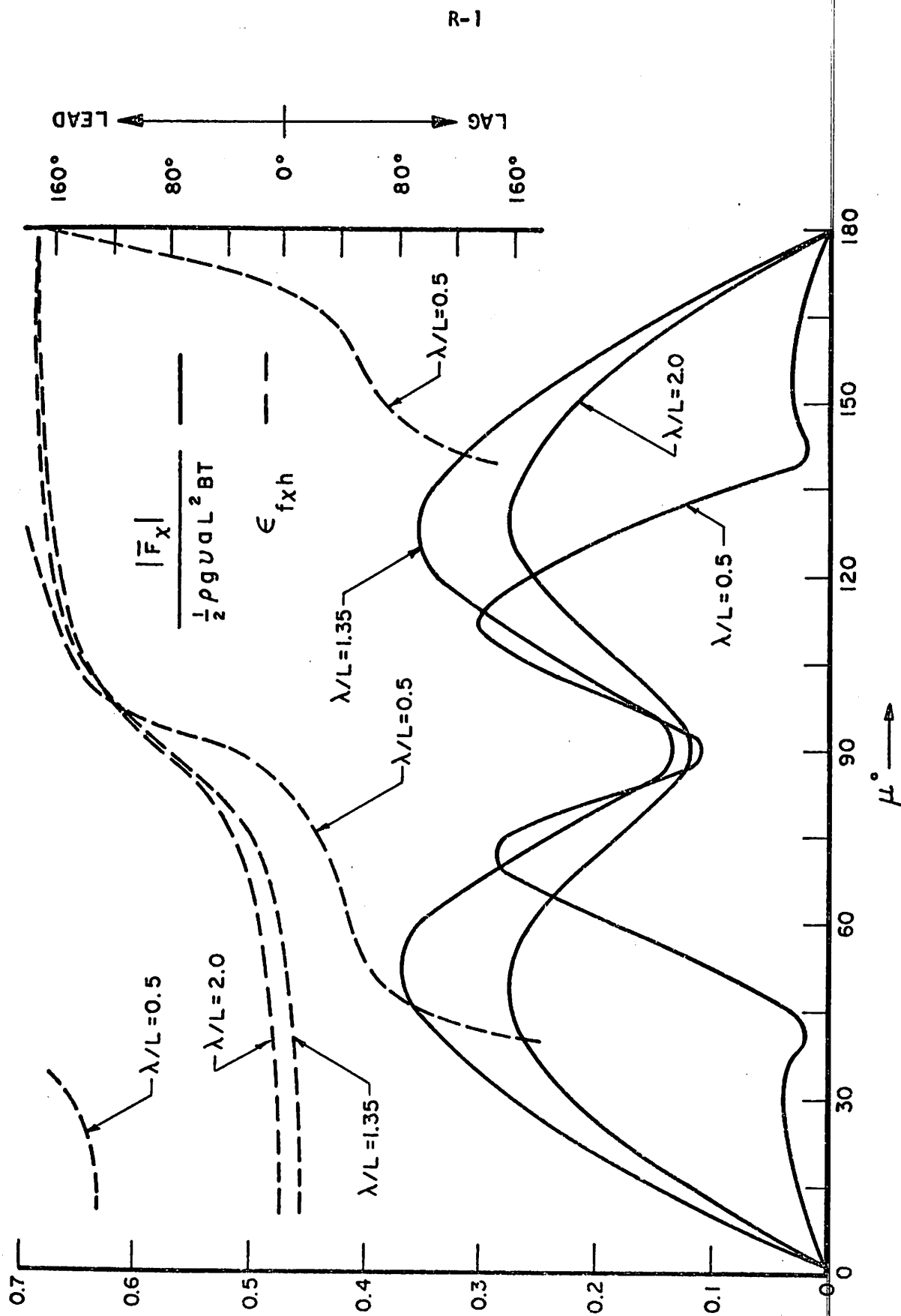


FIG. 10B. YAW-EXCITING MOMENT ON SHIP MODEL IN OBLIQUE SEAS

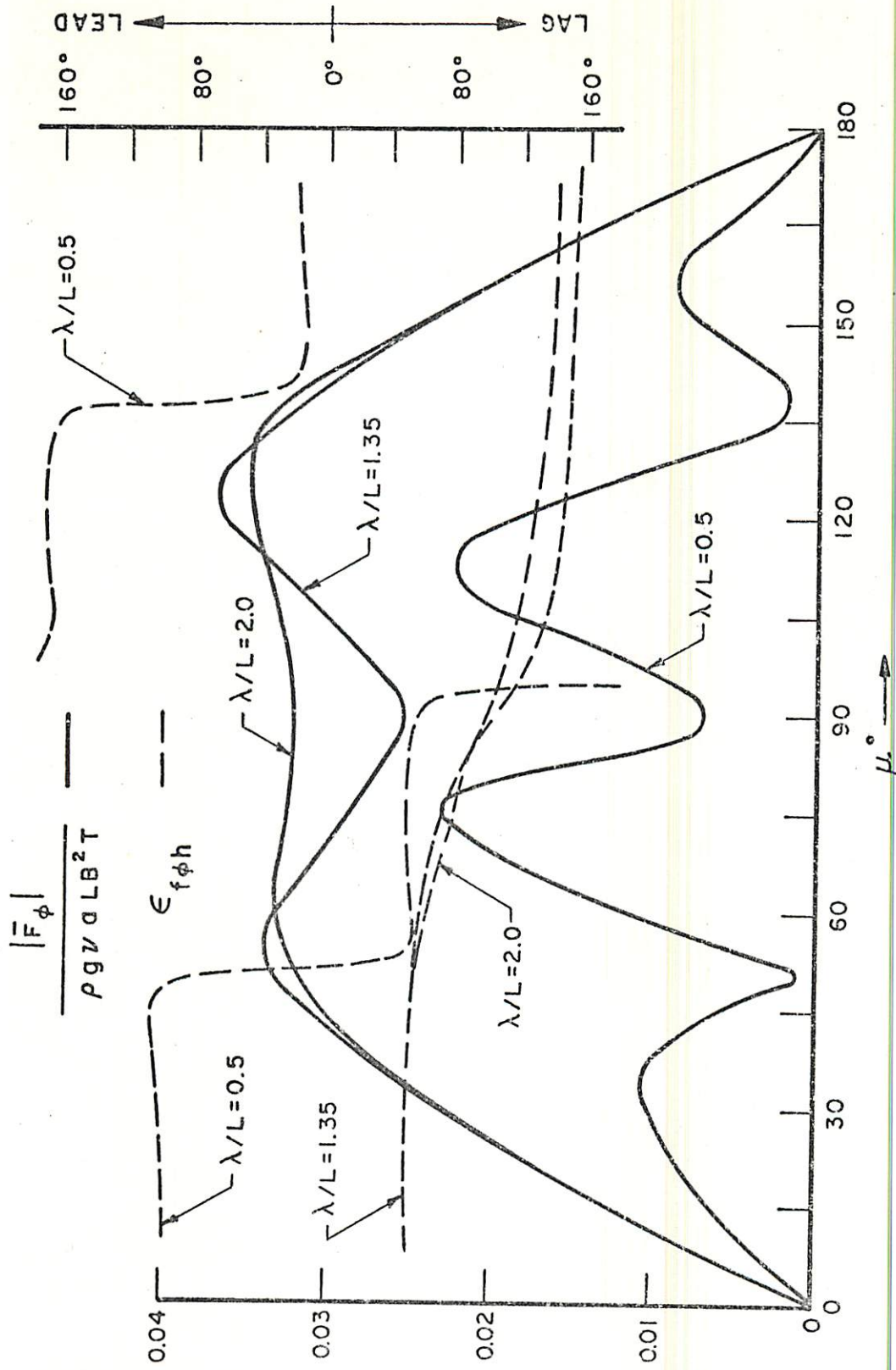


FIG. 10C. ROLL-EXCITING MOMENT ON SHIP MODEL IN OBLIQUE SEAS

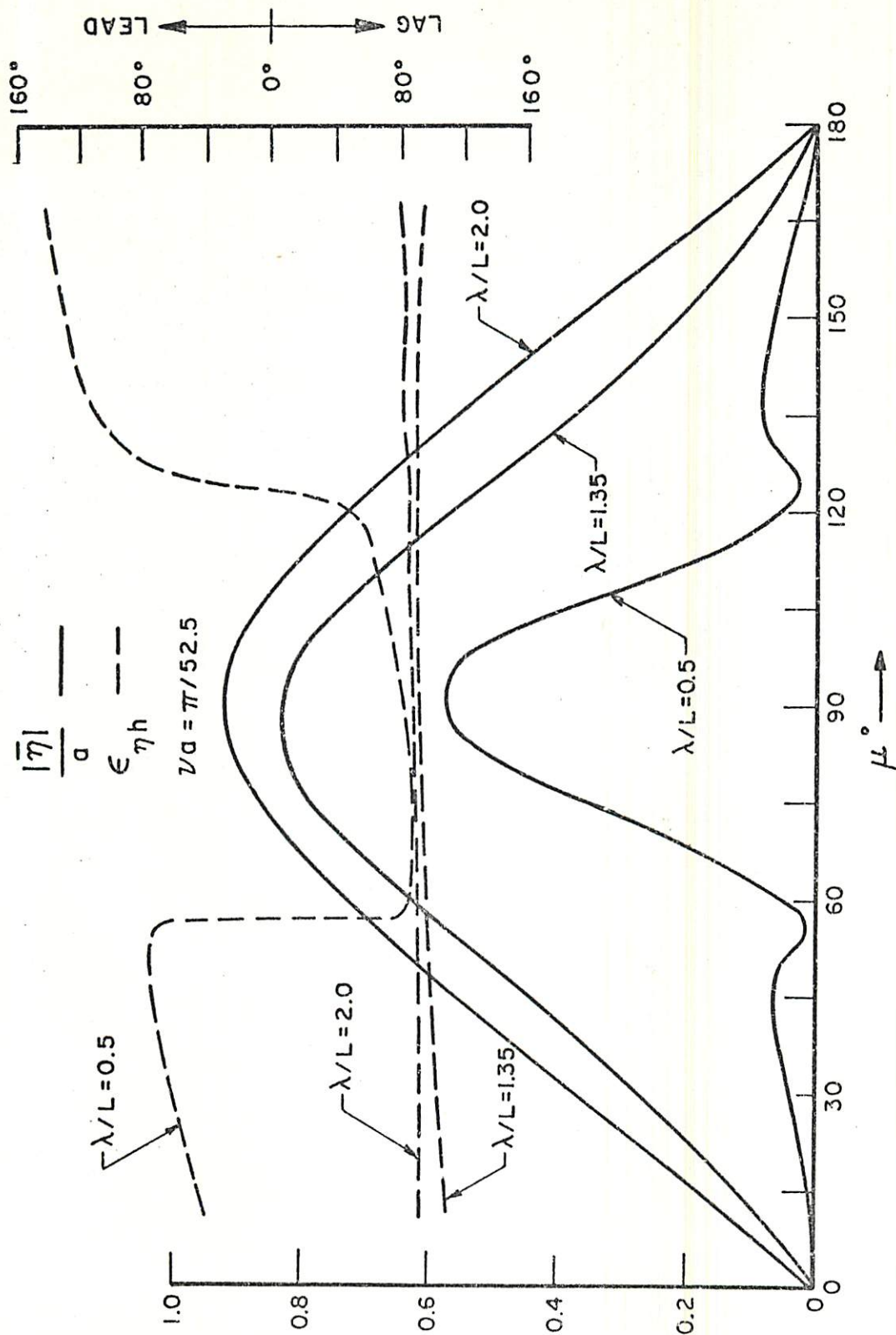


FIG. IIA. SWAYING MOTION OF SHIP MODEL IN OBLIQUE SEAS

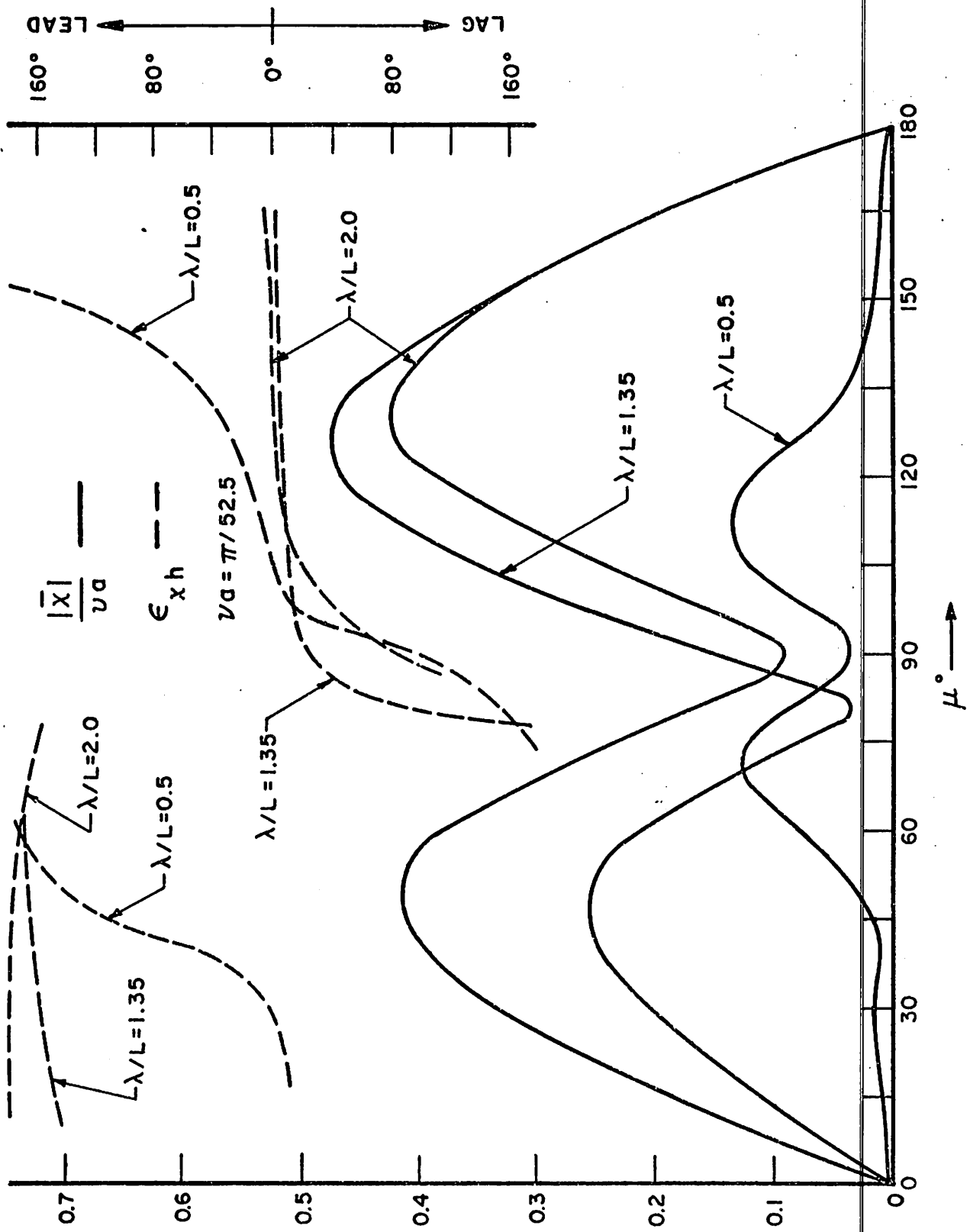


FIG.IIB. YAWING MOTION OF SHIP MODEL IN OBLIQUE SEAS

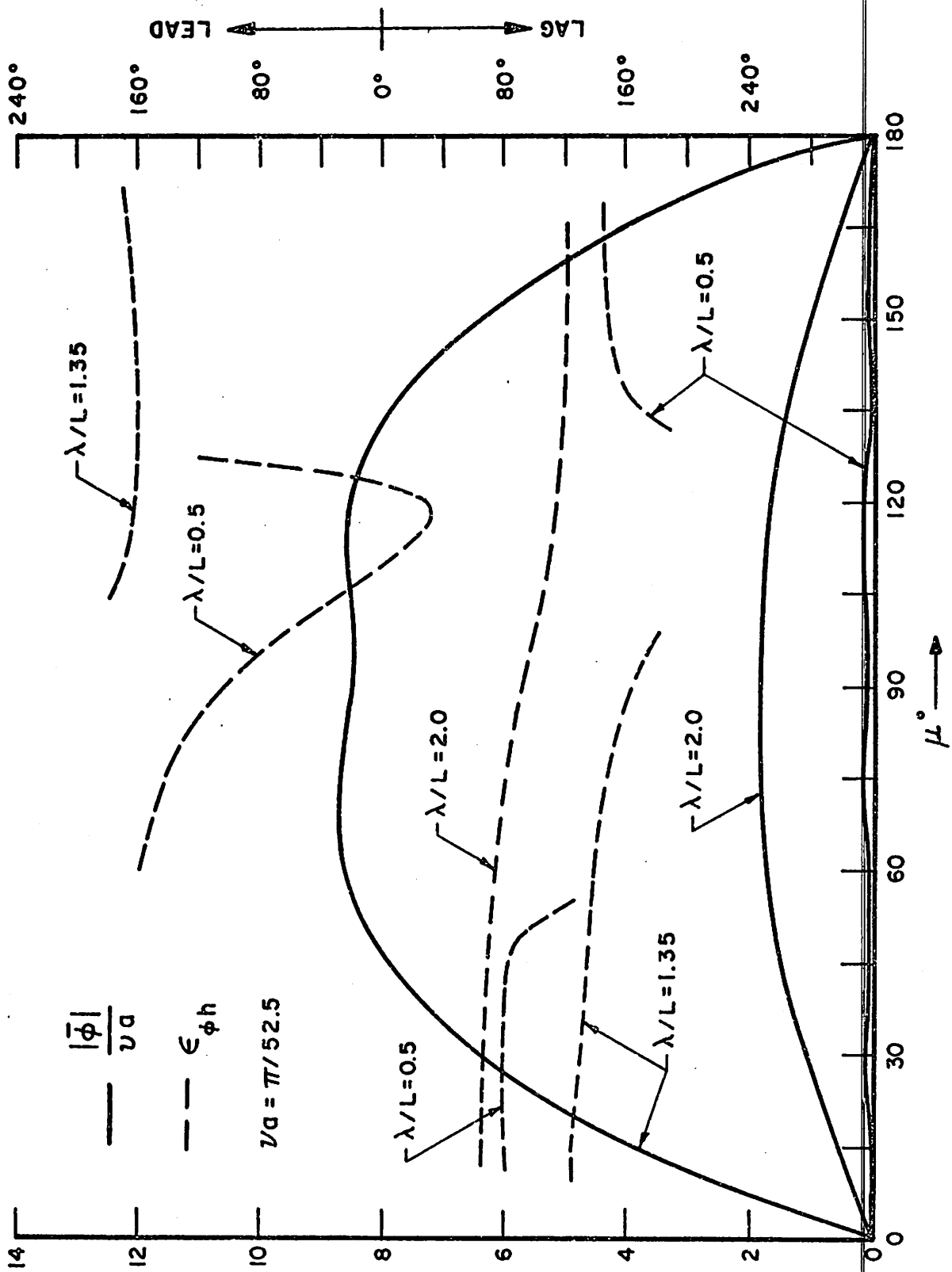


FIG. IIC. ROLLING MOTION OF SHIP MODEL IN OBLIQUE SEAS

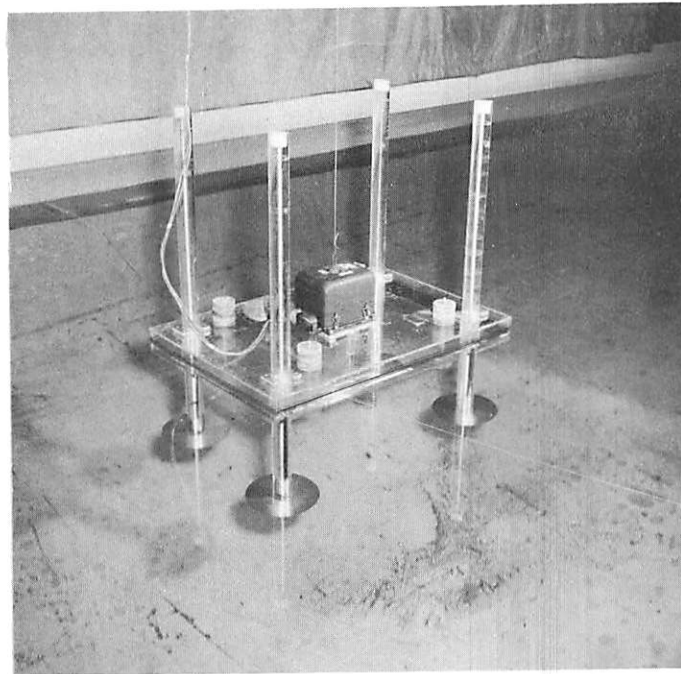


FIG. 12A. JACK UP RIG MODEL WITH LEGS DOWN

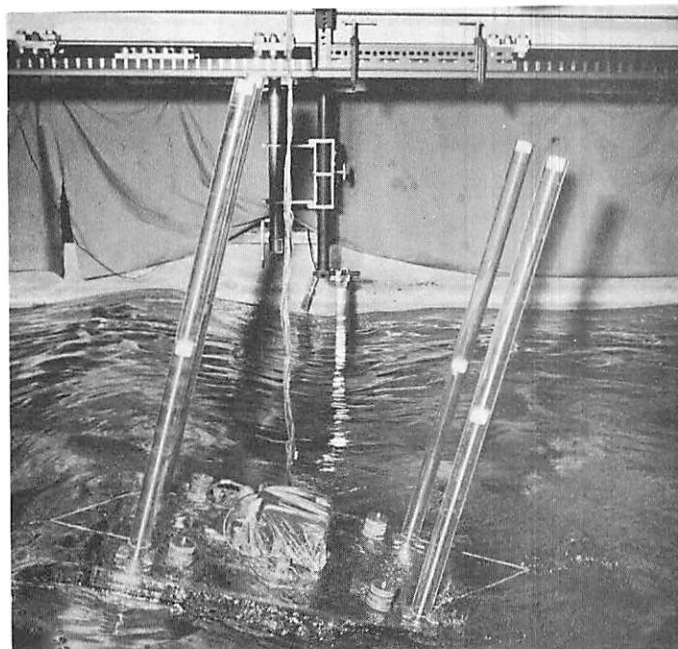


FIG. 12B. JACKUP RIG MODEL WITH LEGS UP IN WAVES

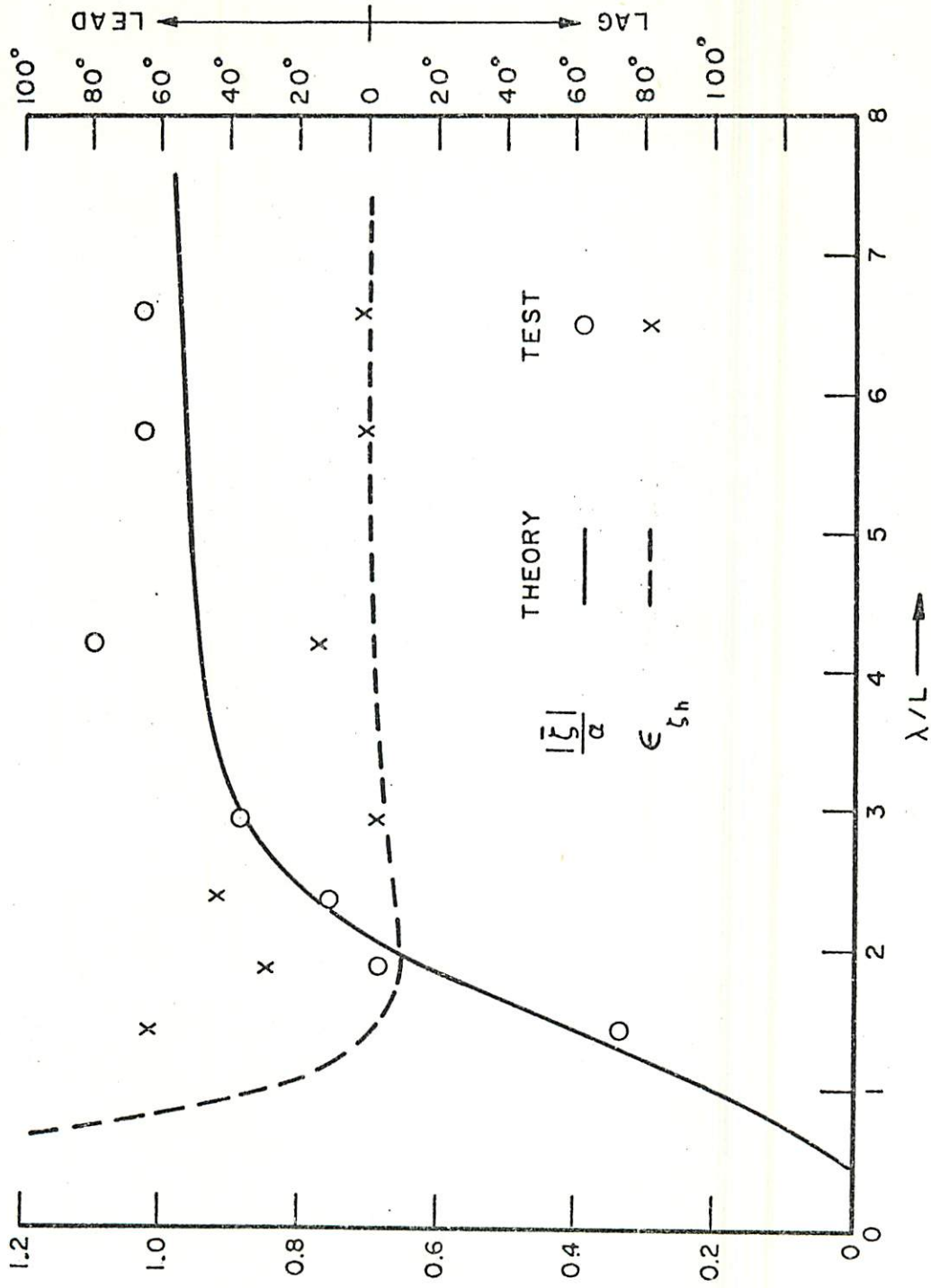


FIG.13A. HEAVING MOTION OF JACK UP RIG MODEL IN HEAD SEAS

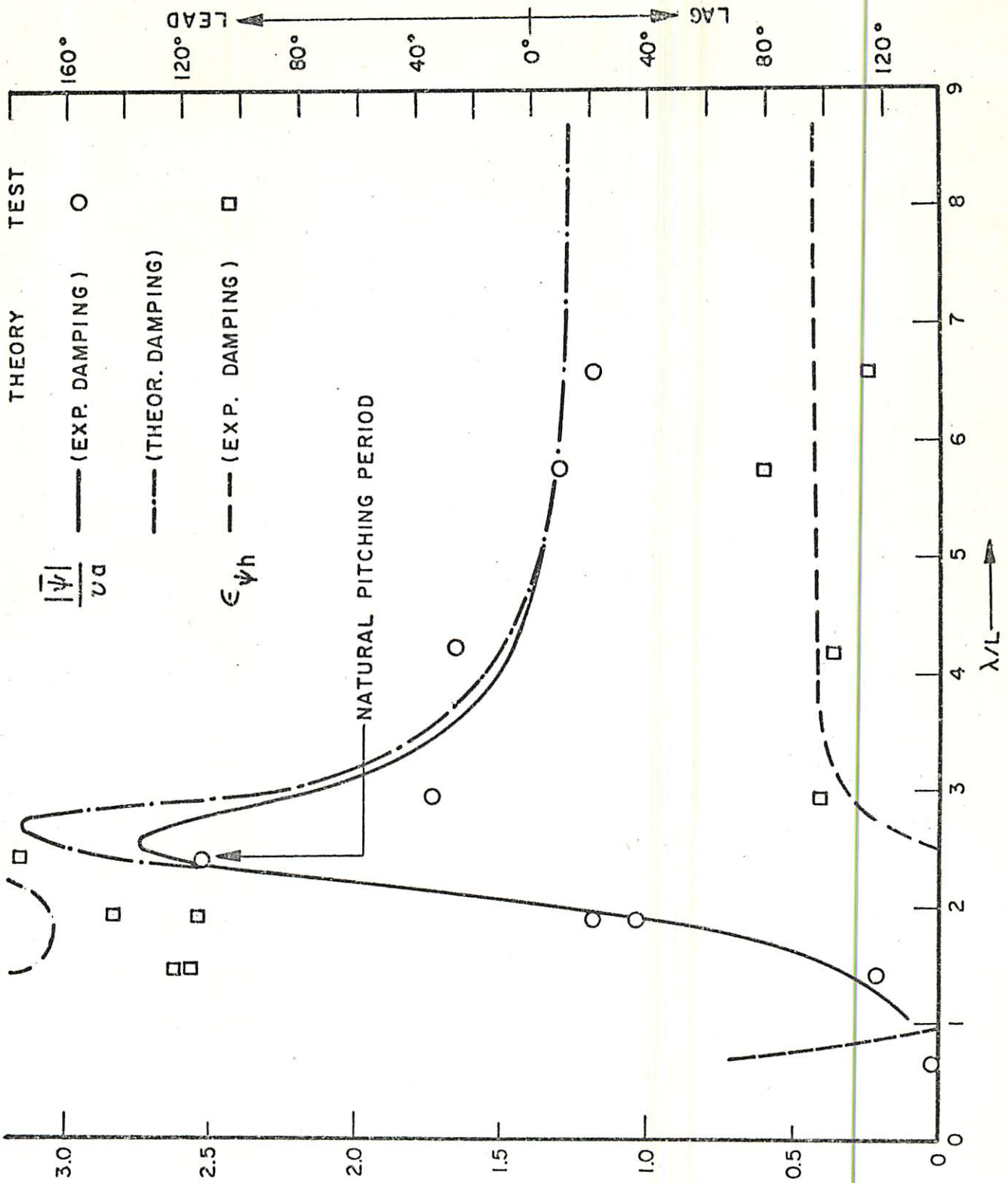


FIG. 13B. PITCHING MOTION OF JACKUP RIG MODEL IN HEAD SEAS

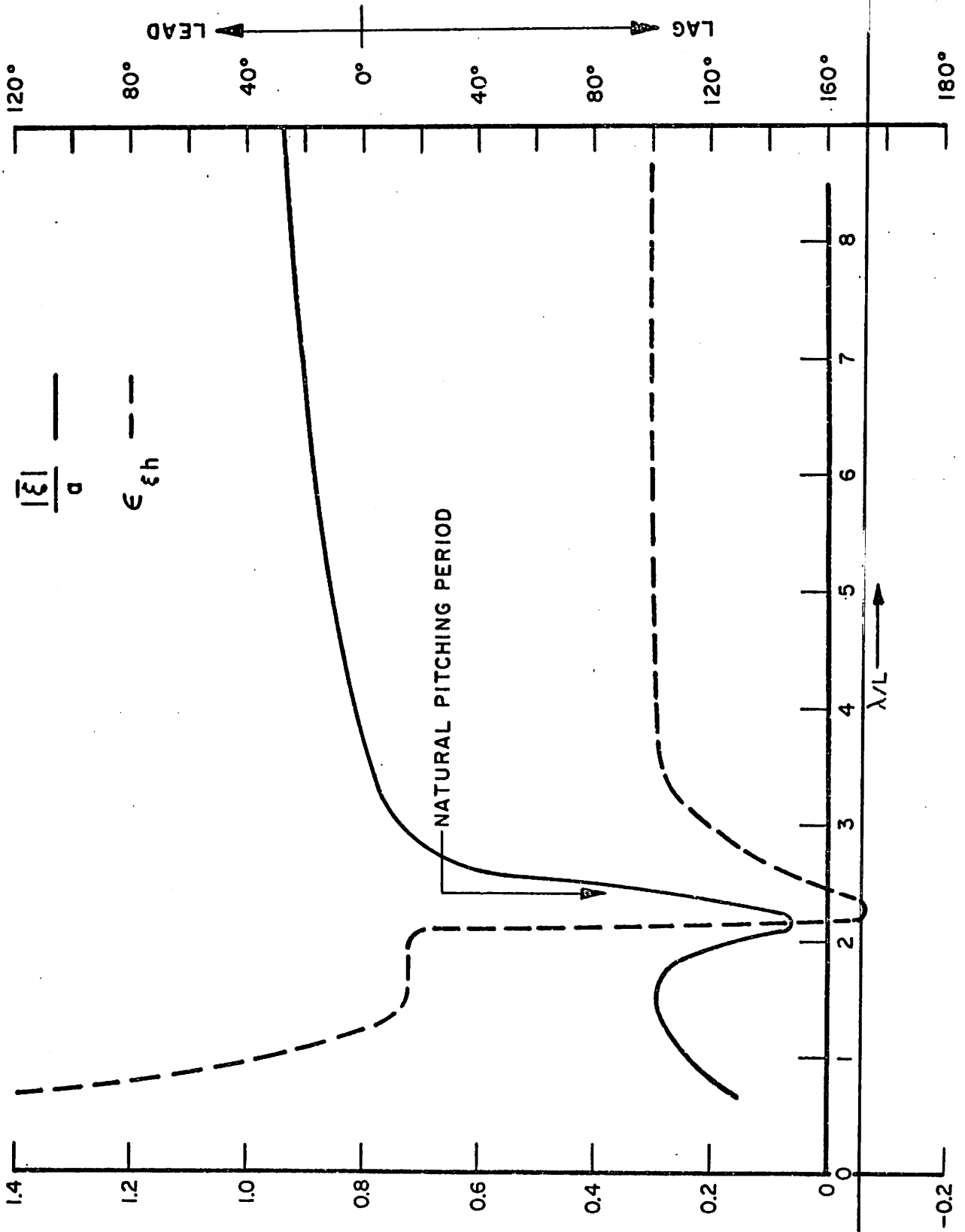


FIG.13C. SURGING MOTION OF JACKUP RIG MODEL IN HEAD SEAS

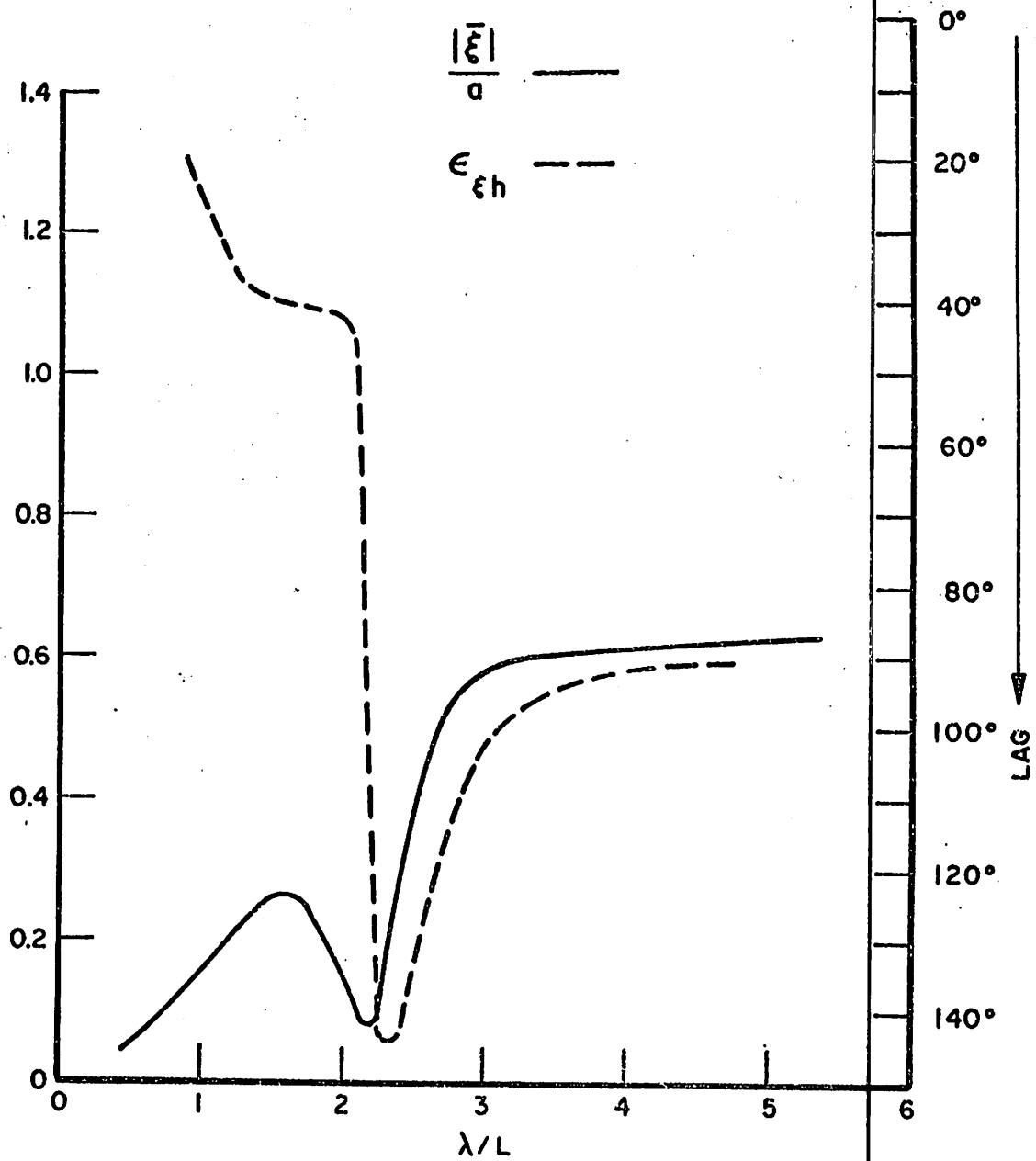


FIG. 14A. SURGING MOTION OF JACKUP RIG MODEL IN QUARTERING SEAS ($\mu = 45^\circ$)

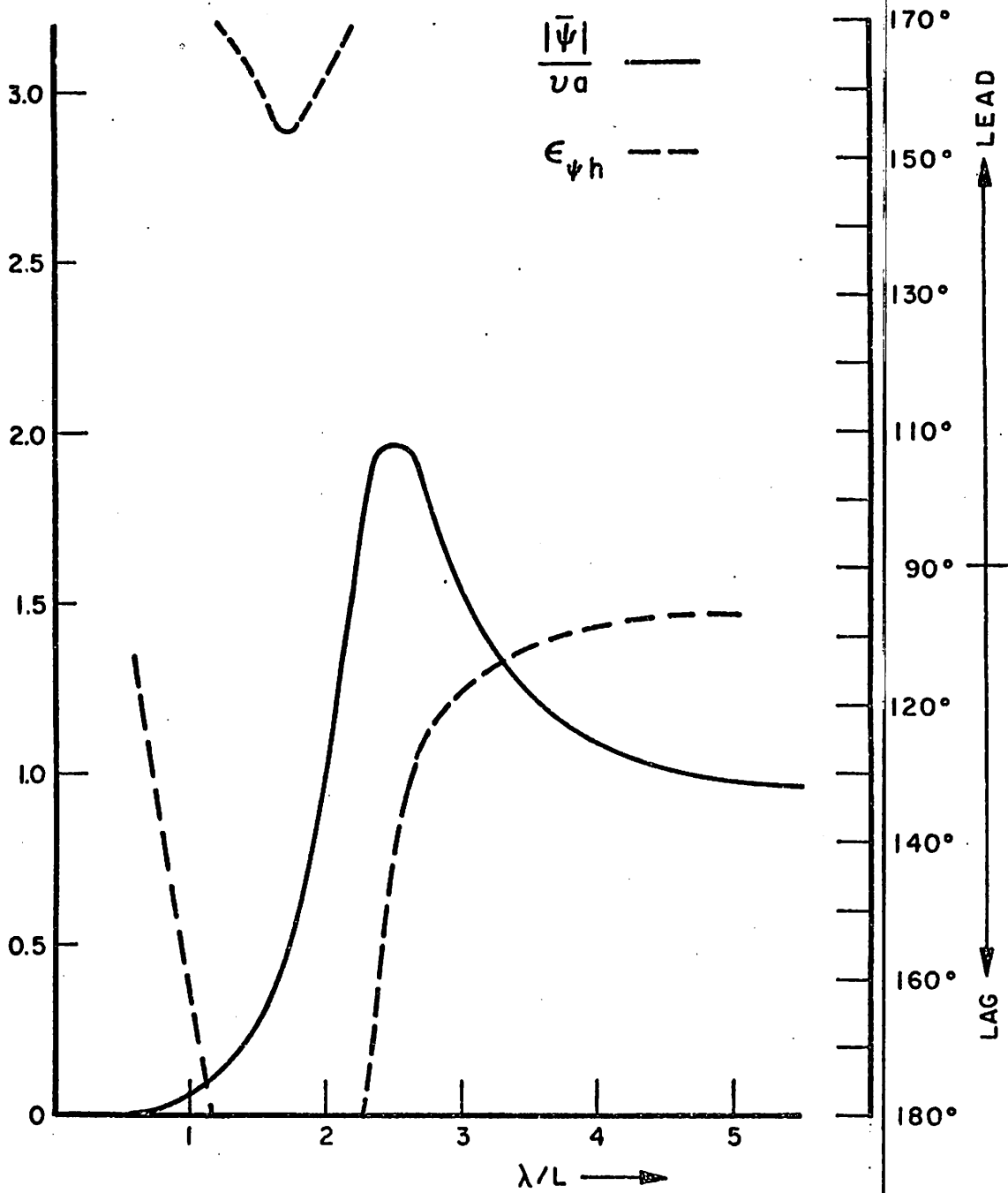


FIG. 14B. PITCHING MOTION OF JACKUP RIG MODEL IN QUARTERING SEAS ($\mu = 45^\circ$)

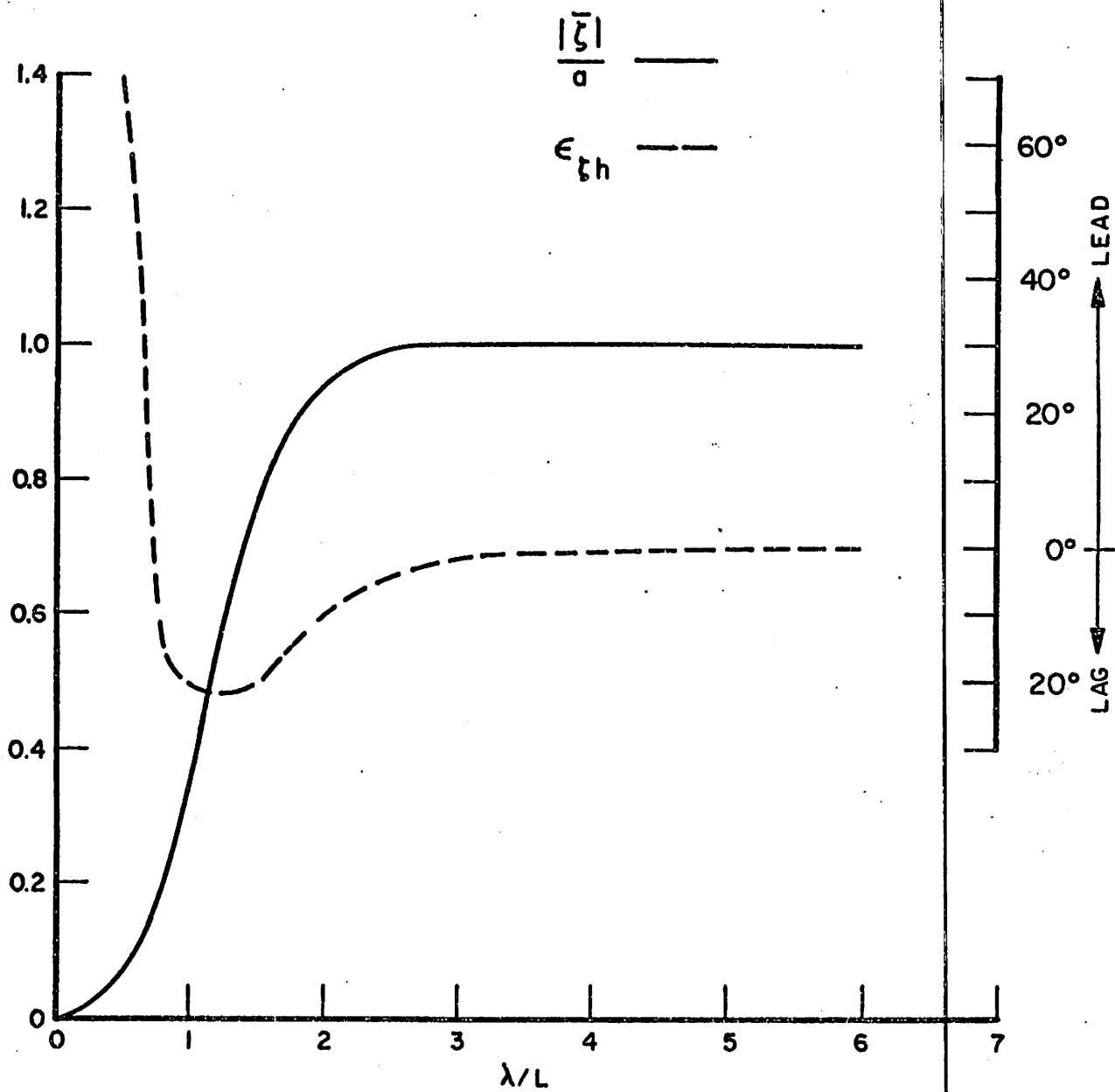


FIG. 15A. HEAVING MOTION OF JACKUP RIG MODEL IN BEAM SEAS ($\mu=90^\circ$)

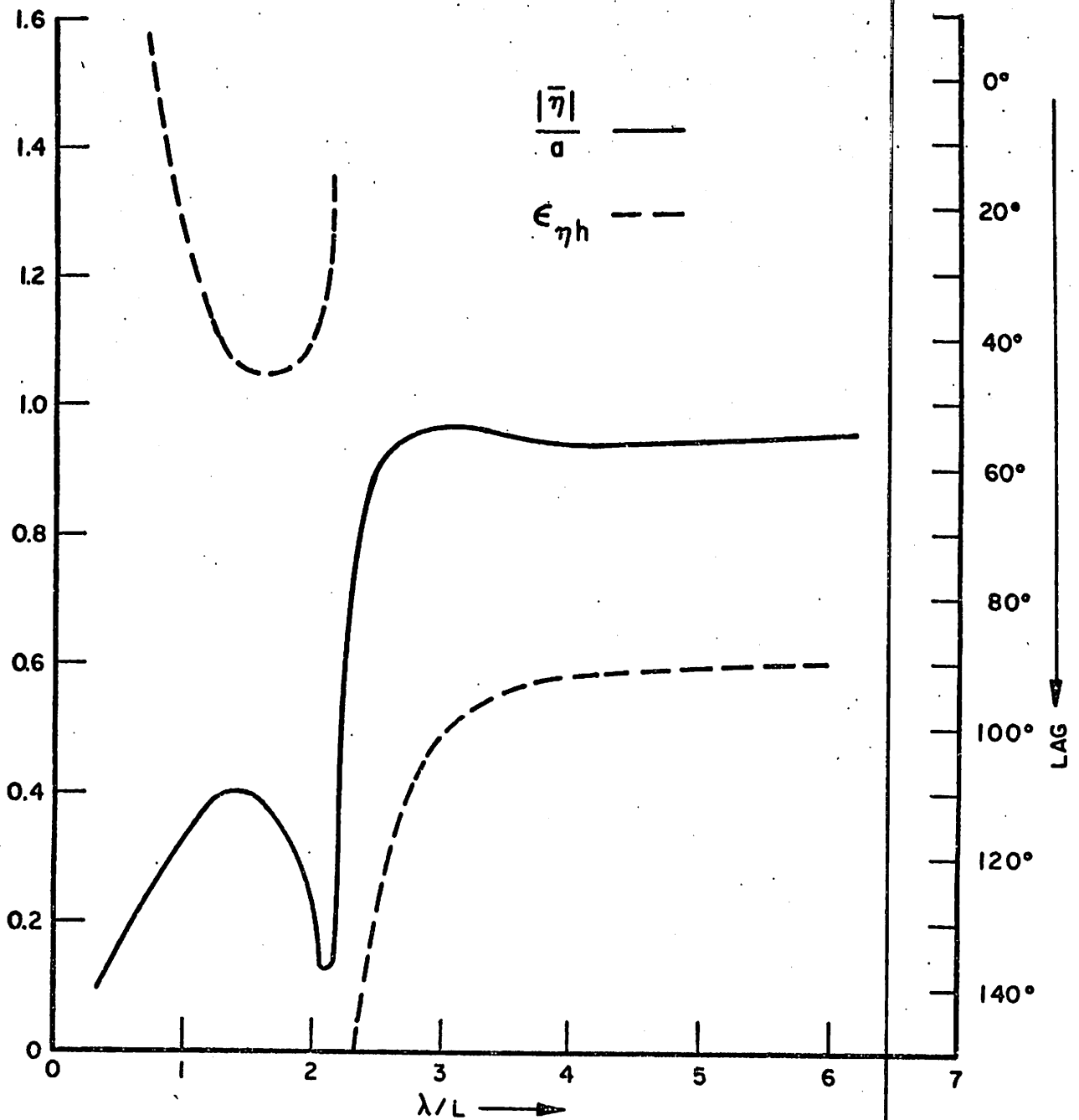


FIG. 15B. SWAYING MOTION OF JACKUP RIG MODEL IN BEAM SEA ($\mu = 90^\circ$)

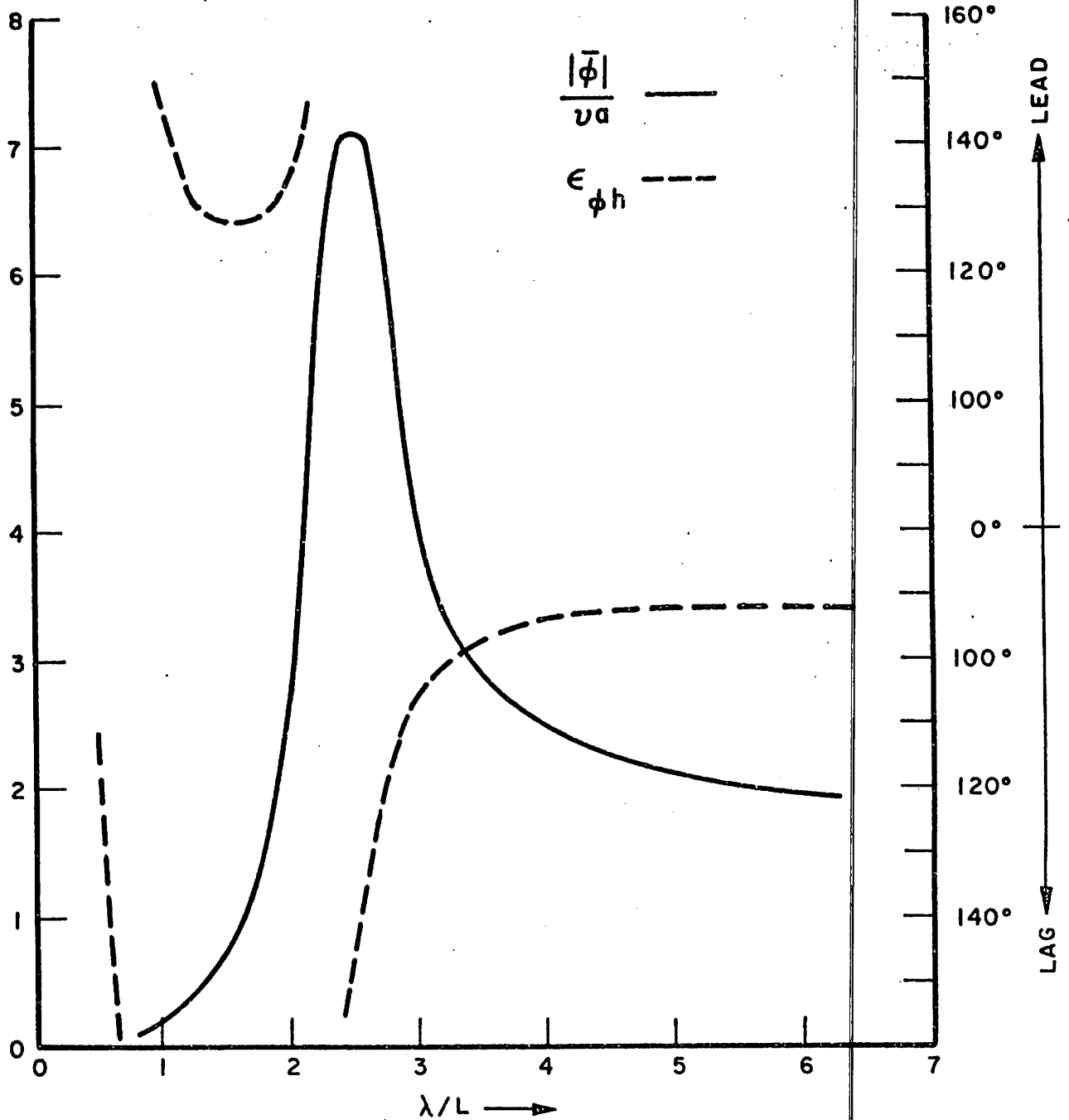


FIG. 15C. ROLLING MOTION OF JACKUP RIG MODEL IN BEAM SEA ($\mu = 90^\circ$)

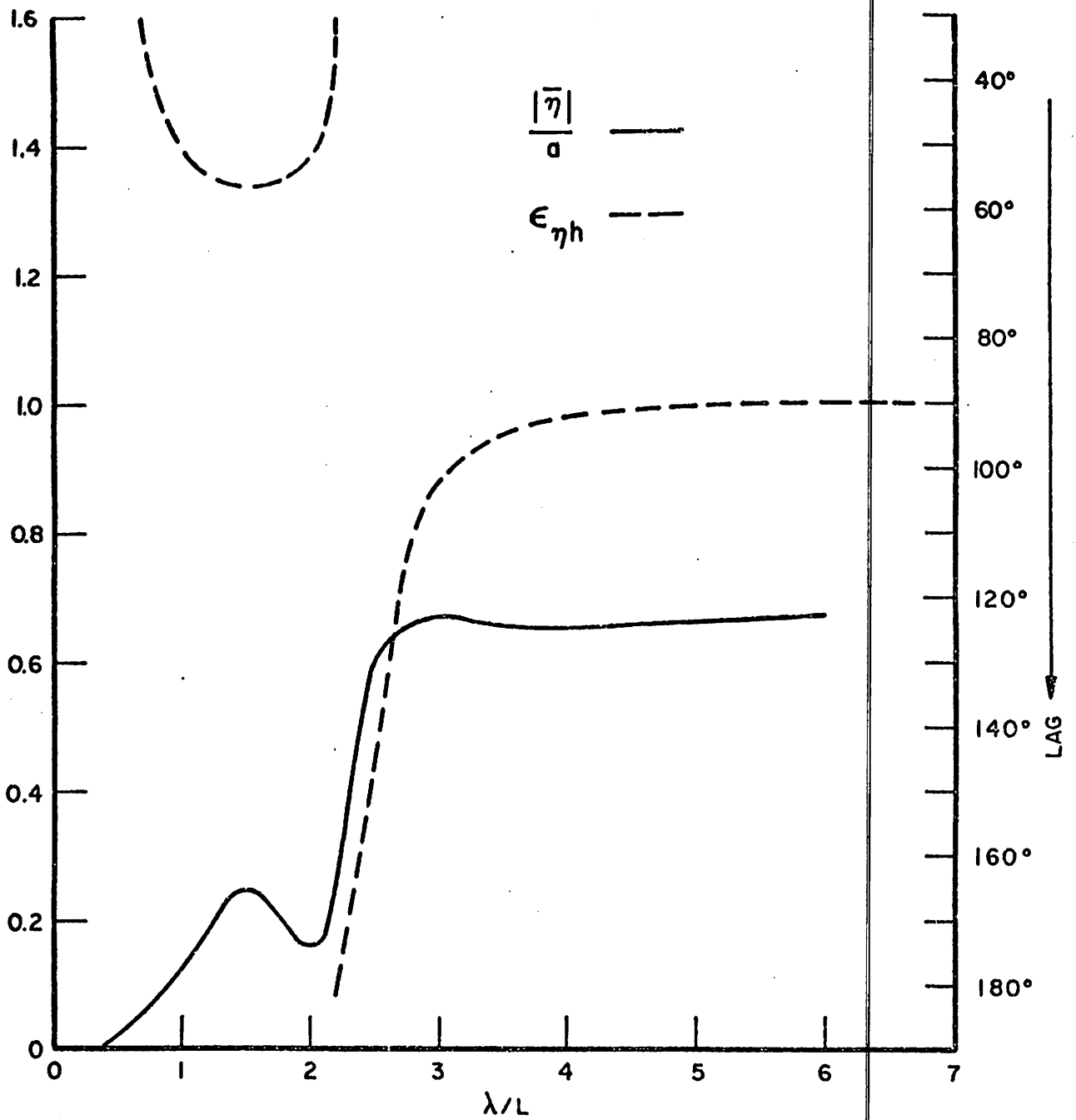


FIG. 16A. SWAYING MOTION OF JACKUP RIG MODEL IN QUARTERING SEAS ($\mu=45^\circ$)

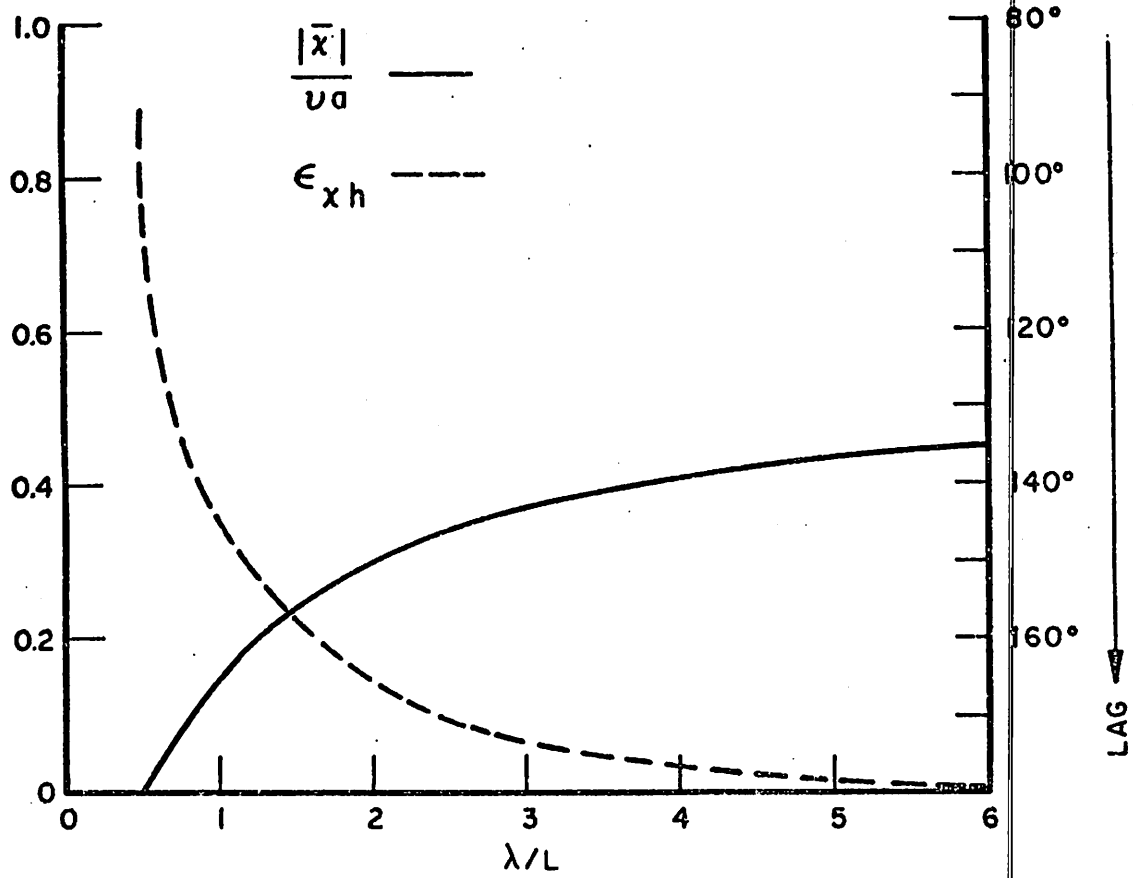


FIG. 16B. YAWING MOTION OF JACKUP RIG MODEL IN QUARTERING SEAS ($\mu = 45^\circ$)

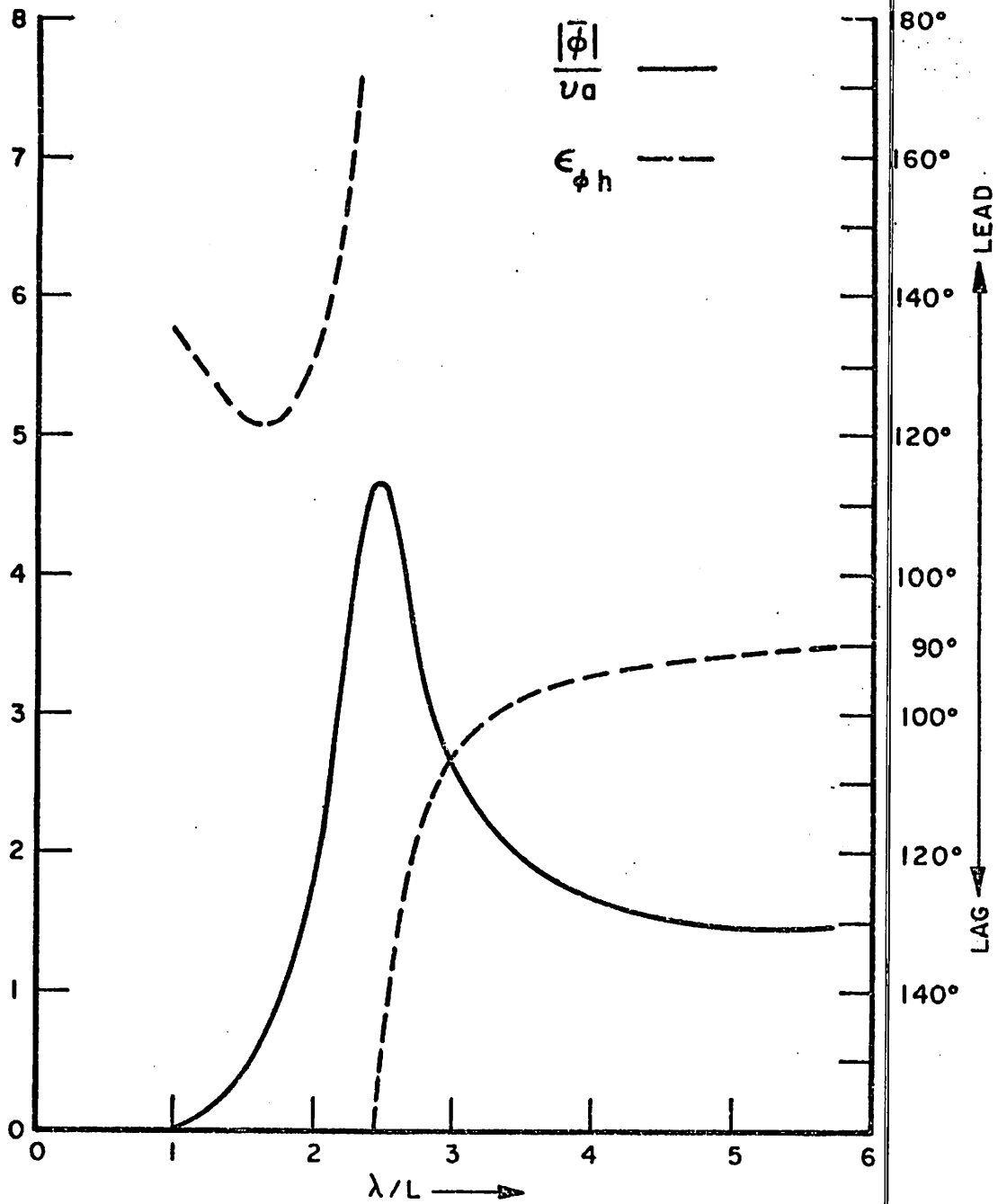


FIG. 16C. ROLLING MOTION OF JACKUP RIG MODEL IN QUARTERING SEAS ($\mu = 45^\circ$)

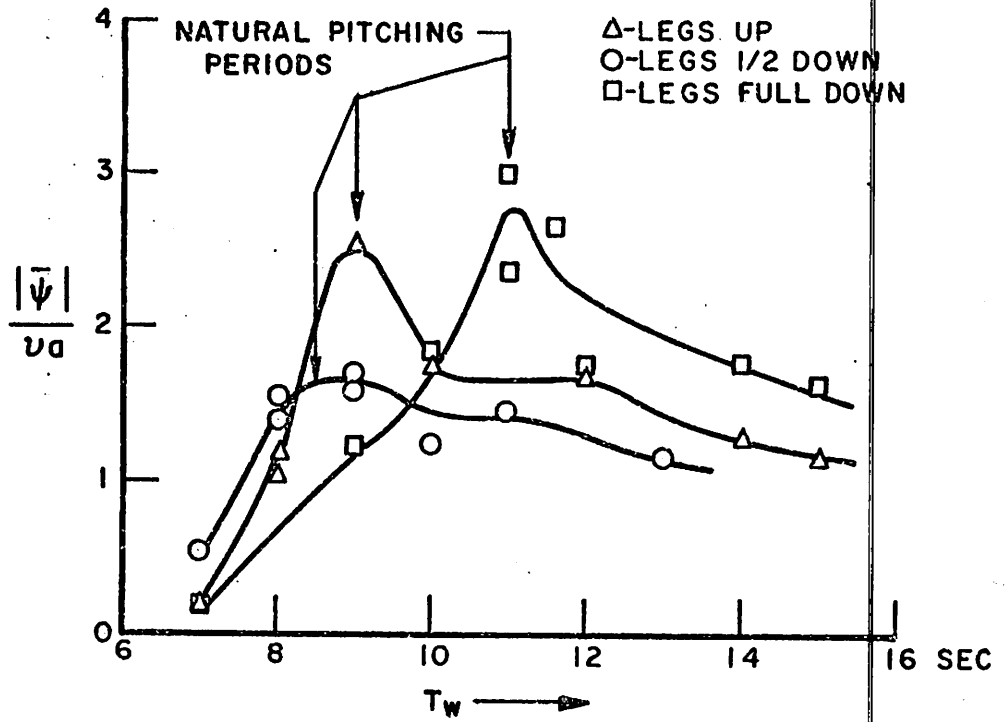


FIG. 17. PITCHING MOTION OF JACKUP RIG PROTOTYPE (SCALE RATIO = 68.5)

Appendix
DIMENSIONLESS FORCE COEFFICIENTS

The inertial and damping coefficients and wave-exciting forces and moments are represented in dimensionless forms, as shown in the tables below.⁸ But the coupled inertial and damping coefficients between heave and pitch, and sway and yaw, are not given.

TABLE A-1

Mode of Motion and Force	Inertial Coefficient	Damping Coefficient
surge → surge	$\frac{M_{\xi\xi}}{\rho \nabla}$	$\frac{N_{\xi\xi} \sqrt{gL}}{\rho g \nabla}$
sway → sway	$\frac{M_{\eta\eta}}{\rho \nabla}$	$\frac{N_{\eta\eta} \sqrt{gL}}{\rho g \nabla}$
heave → heave	$\frac{M_{\zeta\zeta}}{\rho \nabla}$	$\frac{N_{\zeta\zeta} \sqrt{gL}}{\rho g \nabla}$
roll → roll	$\frac{M_{\varphi\varphi}}{\rho \nabla B^2}$	$\frac{N_{\varphi\varphi} \sqrt{gB}}{\rho g \nabla B^2}$
pitch → pitch	$\frac{M_{\psi\psi}}{\rho \nabla L^2}$	$\frac{N_{\psi\psi} \sqrt{gL}}{\rho g \nabla L^2}$
yaw → yaw	$\frac{M_{\chi\chi}}{\rho \nabla L^2}$	$\frac{N_{\chi\chi} \sqrt{gL}}{\rho g \nabla L^2}$
roll → sway	$\frac{M_{\varphi\eta}}{\rho \nabla B}$	$\frac{N_{\varphi\eta} \sqrt{gB}}{\rho g \nabla B}$
sway → roll	$\frac{M_{\eta\varphi}}{\rho \nabla B}$	$\frac{N_{\eta\varphi} \sqrt{gB}}{\rho g \nabla B}$

[cont'd]

Table A-1 (cont'd)

Mode of Motion and Force	Inertial Coefficient	Damping Coefficient
roll \rightarrow yaw	$\frac{M_{\varphi\chi}}{\rho\nabla BL}$	$\frac{N_{\varphi\chi}\sqrt{gB}}{\rho g\nabla BL}$
yaw \rightarrow roll	$\frac{M_{\chi\varphi}}{\rho\nabla BL}$	$\frac{N_{\chi\varphi}\sqrt{gB}}{\rho g\nabla BL}$

TABLE A-2

Mode of Motion	Wave-Exciting Forces
surge	$\frac{\bar{F}_{\xi}}{\rho g\nabla aLBT}$
sway	$\frac{\bar{F}_{\eta}}{\rho g\nabla aLBT}$
heave	$\frac{\bar{F}_{\zeta}}{\rho gaLB}$
roll	$\frac{\bar{F}_{\varphi}}{\rho g\nabla aLB^2T}$
pitch	$\frac{\bar{F}_{\psi}}{\frac{1}{2}\rho gaL^2B}$
yaw	$\frac{\bar{F}_{\chi}}{\frac{1}{2}\rho g\nabla aL^2BT}$

<p>Ocean Engineering Department, Stevens Inst. of Tech. Hoboken, N. J. 07030</p> <p>PREDICTION OF MOTIONS OF OCEAN PLATFORMS IN OBLIQUE SEAS</p> <p>C. H. Kim and F. Chou. Report SIT-0E-70-1. June 1970. xiii + 78 pp., 1 appendix, 17 figures.</p> <p>This investigation was supported in part by the National Science Foundation, under NSF/Sea Grant GH-60. Requests for copies of the report should be addressed to the Clearinghouse for Scientific and Technical Information, 5285 Port Royal Road, Springfield, Virginia 22151.</p> <p>(SIT-0E Project 3617/458).</p>	<p>Ocean Engineering Department, Stevens Inst. of Tech. Hoboken, N. J. 07030</p> <p>PREDICTION OF MOTIONS OF OCEAN PLATFORMS IN OBLIQUE SEAS</p> <p>C. H. Kim and F. Chou. Report SIT-0E-70-1. June 1970. xiii + 78 pp., 1 appendix, 17 figures.</p> <p>This investigation was supported in part by the National Science Foundation, under NSF/Sea Grant GH-60. Requests for copies of the report should be addressed to the Clearinghouse for Scientific and Technical Information, 5285 Port Royal Road, Springfield, Virginia 22151.</p> <p>(SIT-0E Project 3617/458).</p>
<p>Ocean Engineering Department, Stevens Inst. of Tech. Hoboken, N. J. 07030</p> <p>PREDICTION OF MOTIONS OF OCEAN PLATFORMS IN OBLIQUE SEAS</p> <p>C. H. Kim and F. Chou. Report SIT-0E-70-1. June 1970. xiii + 78 pp., 1 appendix, 17 figures.</p> <p>This investigation was supported in part by the National Science Foundation, under NSF/Sea Grant GH-60. Requests for copies of the report should be addressed to the Clearinghouse for Scientific and Technical Information, 5285 Port Royal Road, Springfield, Virginia 22151.</p> <p>(SIT-0E Project 3617/458).</p>	<p>Ocean Engineering Department, Stevens Inst. of Tech. Hoboken, N. J. 07030</p> <p>PREDICTION OF MOTIONS OF OCEAN PLATFORMS IN OBLIQUE SEAS</p> <p>C. H. Kim and F. Chou. Report SIT-0E-70-1. June 1970. xiii + 78 pp., 1 appendix, 17 figures.</p> <p>This investigation was supported in part by the National Science Foundation, under NSF/Sea Grant GH-60. Requests for copies of the report should be addressed to the Clearinghouse for Scientific and Technical Information, 5285 Port Royal Road, Springfield, Virginia 22151.</p> <p>(SIT-0E Project 3617/458).</p>